Computers, Materials & Continua

Tech Science Press

https://doi.org/10.32604/cmc.2026.080581

REVIEW

Physics-Based Modelling of Plasma-Material Interactions and Phase Transformations in Electrical Discharge Machining: A Computational Materials Perspective

Kamlesh Paswan[1], Rajnish Singh[2], Vivekanand Singh[3], Brihaspati Singh[4], Ankur Saxena[5] and Chandrmani Yadav[6,*]

[1]Department of Mechanical Engineering, Galgotias University, Greater Noida, India
[2]Department of Mechanical Engineering, Kamla Nehru Institute of Technology, Sultanpur, India
[3]Rajkiya Engineering College, Ambedkar Nagar, Uttar Pradesh, India
[4]Department of Mechanical Engineering, Rajkiya Engineering College, Azamgarh, India
[5]Department of Electronics and Communication Engineering, University Institute of Emerging and Technologies, Guru Nanak University, Ibrahimpatnam, Hyderabad, India
[6]Marwadi University Research Centre, Department of Mechanical Engineering, Faculty of Engineering & Technology, Marwadi University, Rajkot, India

*Corresponding Author: Chandrmani Yadav. Email: yadavchandrmani@gmail.com

Received: 25 February 2026; Accepted: 30 April 2026; Published: 15 June 2026

ABSTRACT: Electrical Discharge Machining (EDM) is governed by highly coupled, nonlinear electro-thermal-mechanical phenomena involving plasma-mediated energy transfer, rapid heat conduction, phase transformation, and resolidification over micro to nanosecond time scales. From a computational materials science perspective, EDM serves as a prototypical problem of extreme, localised energy–matter interaction, where predictive modelling requires rigorous treatment of multiphysics coupling and scale bridging. This review presents a critical synthesis of theoretical and numerical frameworks for modelling advanced EDM configurations, including vibration-assisted and turning-based EDM, powder- and nano-additive-assisted EDM, and alternative dielectric environments. The review consolidates continuum-based formulations that describe the evolution of the electric field, plasma channel dynamics, and transient heat transfer, typically governed by Maxwell's equations coupled with Fourier and non-Fourier heat conduction models. Thermo-fluid and thermo-mechanical models accounting for melt flow, recoil pressure, surface tension, and thermal stress evolution are analysed for their ability to predict crater geometry, recast layer formation, and subsurface damage. The influence of externally imposed perturbations such as mechanical vibration, relative rotational kinematics, and particle-mediated plasma modulation is discussed through modifications in boundary conditions, energy partition coefficients, and effective transport properties. Multiscale modelling strategies that bridge discharge-scale plasma physics with mesoscale thermal fields and microscale material response are critically reviewed, including hybrid finite element–finite volume schemes and reduced-order models. In parallel, data-driven surrogate models and machine learning approaches are examined for parameter inference, uncertainty reduction, and rapid prediction of material behaviour. Major challenges related to model closure, scale separation, and experimental validation are identified, and future research directions are outlined toward fully coupled multiscale and digital twin frameworks for predictive EDM-induced material response.

KEYWORDS: Electrical discharge machining; plasma–material interaction; multiphysics and multiscale modelling; phase transformation; thermo-mechanical effects; machine learning-assisted EDM

1 Introduction

Electrical Discharge Machining (EDM) is fundamentally governed by highly localised, transient plasma–material interactions in which extreme energy densities are delivered to the workpiece surface over microsecond timescales. A material removal in EDM does not occur through conventional mechanical deformation, but rather through a sequence of dielectric breakdown, plasma channel formation, intense Joule heating, and rapid melting and vaporisation of the electrode–workpiece interface. The discharge plasma, characterised by temperatures exceeding 1000 K and steep thermal gradients, induces non-equilibrium phase transformations, solidification, and the formation of a recast layer with altered microstructural and thermophysical properties [1,2]. Despite decades of industrial application, the underlying physics of energy transfer from the plasma to the solid, the partitioning of discharge energy, and the coupling between thermal, electromagnetic, and phase-change phenomena remain only partially understood. This complexity has motivated the development of physics-based and computational models capable of capturing plasma evolution, transient heat flux distribution, and material response at micro- and sub-micro scales [3]. Klocke et al. [4] investigated temperature fields and power distribution in EDM, overcoming the impracticality of direct thermal measurements near the discharge zone. Experiments with a copper tool electrode measured internal temperatures, which were matched using a coupled thermo-fluid finite element method (FEM) model in COMSOL. By fitting simulations to experiments, the study determined that 49% of the discharge energy dissipates into the tool electrode and that flushing velocity significantly affects thermal behaviour.

EDM has evolved significantly from its early reliance on empirical parameter tuning toward a more sophisticated, physics-informed understanding of the process. Conventional EDM approaches were largely based on trial-and-error optimisation and simplified discharge theories, offering limited insight into the underlying plasma–material interactions, transient heat transfer, and phase transformation mechanisms that govern material removal and surface integrity. As a result, early models were typically single-physics and machine-specific, exhibiting poor generalizability across materials and operating conditions [5,6]. Fig. 1 illustrates the evolution of technology in EDM from conventional practices to advanced methodologies. Recent reviews emphasise that such empirical frameworks are insufficient to capture the highly stochastic, nonlinear, and coupled nature of EDM discharges, particularly for advanced materials and precision applications [7,8].

Figure 1: Technology evolution in EDM from conventional to recent advances.

In response, recent EDM research has shifted toward physics-based, multiphysics, and data-assisted methodologies, integrating finite element and computational fluid dynamics models with artificial intelligence (AI) and hybrid process strategies. Advances in multiphysics modelling now enable partial representation of plasma channel evolution, thermal–fluid coupling, and melt pool dynamics. At the same time, hybrid and AI-assisted approaches support multi-objective optimisation and adaptive control [9,10]. Moreover, emerging trends such as micro-/nano-EDM, hybrid EDM processes, green EDM, and digital twin concepts reflect a broader transition toward predictive, sustainable, and intelligent manufacturing systems. These developments collectively underscore the growing need for multiscale, physics-informed modelling frameworks capable of bridging plasma-scale phenomena with material-scale phase transformations, thereby forming the foundation for next-generation EDM research and applications [11,12].

Recent studies have employed advanced diagnostics, experimental design, and hybrid manufacturing approaches to deepen understanding of EDM mechanisms and to optimise performance. High-resolution plasma diagnostics combining optical emission spectroscopy (OES) with collisional–radiative (CR) modelling, supported by high-speed imaging and electrical signal analysis, have revealed that EDM discharges in both liquid (oil) and gaseous (air) dielectrics exhibit comparable electron temperatures, reaching approximately 15,000 K in the plasma plume and 21,000 K in the hot spot. However, electron densities during discharge initiation were found to be up to eight times higher in oil. At the same time, plasma composition differed significantly: air discharges were dominated by electrode-material species. In contrast, oil-based plasmas were rich in hydrogen and carbon originating from dielectric decomposition, highlighting fundamentally different plasma–material interaction pathways [13].

The infographic, shown in Fig. 2, illustrates the complementary roles of FEM models, molecular dynamics (MD) models, and flow-field models in advancing the modelling of the EDM process. FEM-based models primarily address macroscopic thermal and electrical phenomena, enabling the prediction of temperature distributions, heat-affected zones (HAZ), crater geometry, and overall machining performance through assumed heat-source formulations, such as Gaussian heat-flux distributions. These models are widely used to estimate material removal rate, tool wear, and surface integrity. Still, they are limited in their ability to resolve atomistic-scale phase transitions and plasma–material interaction mechanisms [14].

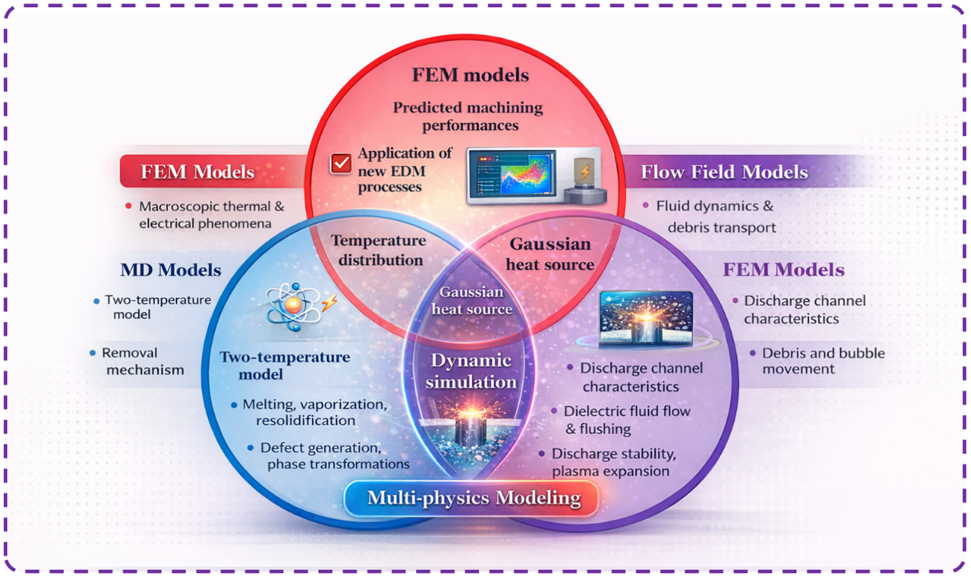

Figure 2: Integrated modelling framework for EDM.

MD models focus on microscale and atomistic phenomena governing material-removal mechanisms, including melting, vaporisation, solidification, and defect generation under extreme thermal gradients. Approaches such as the two-temperature model (TTM) enable separation of electron and lattice temperatures, providing insight into ultrafast energy transfer and phase transformations that cannot be captured by continuum methods alone. However, MD simulations are computationally expensive and restricted to small spatial and temporal domains, limiting their direct applicability to full-scale EDM processes [15,16].

Flow field models, typically based on computational fluid dynamics (CFD), describe the dynamics of the discharge channel, dielectric fluid motion, debris transport, and bubble evolution, which critically influence discharge stability, plasma expansion, and flushing efficiency. The overlap between FEM and flow-field models enables the dynamic simulation of plasma heat sources. At the same time, integration across all three modelling approaches yields multiphysics frameworks capable of coupling thermal, electrical, fluid, and material responses. Such integrated models form the foundation for next-generation EDM simulation strategies, supporting the development of new EDM processes and enabling more reliable predictions of machining outcomes through multiphysics and multiscale modelling [17,18].

Furthermore, a bibliometric analysis was conducted in accordance with Preferred Reporting Items for Systematic Review and Meta-Analysis (PRISMA) guidelines [19] to ensure clarity, accuracy, and reproducibility. Fig. 3 shows the flowchart of the adopted approach. In this analysis, the Scopus database was used as the primary source of information. It was selected due to its extensive coverage of engineering and technology articles, reliable metadata, and strong citation tracking capabilities. A structured search strategy was developed using Boolean operators to identify relevant studies, incorporating keywords such as EDM, plasma, and dielectric breakdown phenomena, plasma–material and energy–matter interactions, physics-based and mechanistic modeling approaches, phase transformation mechanisms, and computational material simulations (e.g., FEM and CFD). The search was limited to publications from 2015 to 2025, including research articles, review papers, and conference proceedings, while excluding book chapters, books, editorials, short surveys, and retracted publications. Additionally, only English-language publications were considered to ensure consistency and quality.

Fig. 4a illustrates the annual publication trend, showing a steady, pronounced increase in research output, rising from approximately 500 documents in 2015 to nearly 3700 in 2025, corresponding to an average annual growth rate of about 22%. This trend highlights the rapidly growing interest in physics-based and Multiphysics modelling of plasma-assisted material removal and phase-change phenomena in EDM.

Fig. 4b depicts the distribution of document types, where journal articles dominate (74.6%), followed by review papers (16.7%), indicating a mature and well-established research field supported by both fundamental and synthesis-oriented studies. Conference papers, book chapters, and books together account for a smaller yet meaningful share, reflecting ongoing dissemination of emerging computational and modelling techniques.

Fig. 4c shows the geographical distribution of publications, with China emerging as the leading contributor, followed by the United States, India, Germany, and the United Kingdom. This global distribution underscores widespread international efforts in advancing plasma–material interaction modelling and computational materials research related to EDM.

Fig. 4d presents the subject-area classification, revealing that Materials Science (27.2%) and Engineering (21.6%) dominate the articles, followed by Physics and Astronomy (17.6%) and Chemistry (8.7%). The strong presence of physics- and materials-oriented disciplines confirms the inherently multidisciplinary nature of EDM research, bridging plasma physics, non-equilibrium phase transformations, and computational materials modelling frameworks.

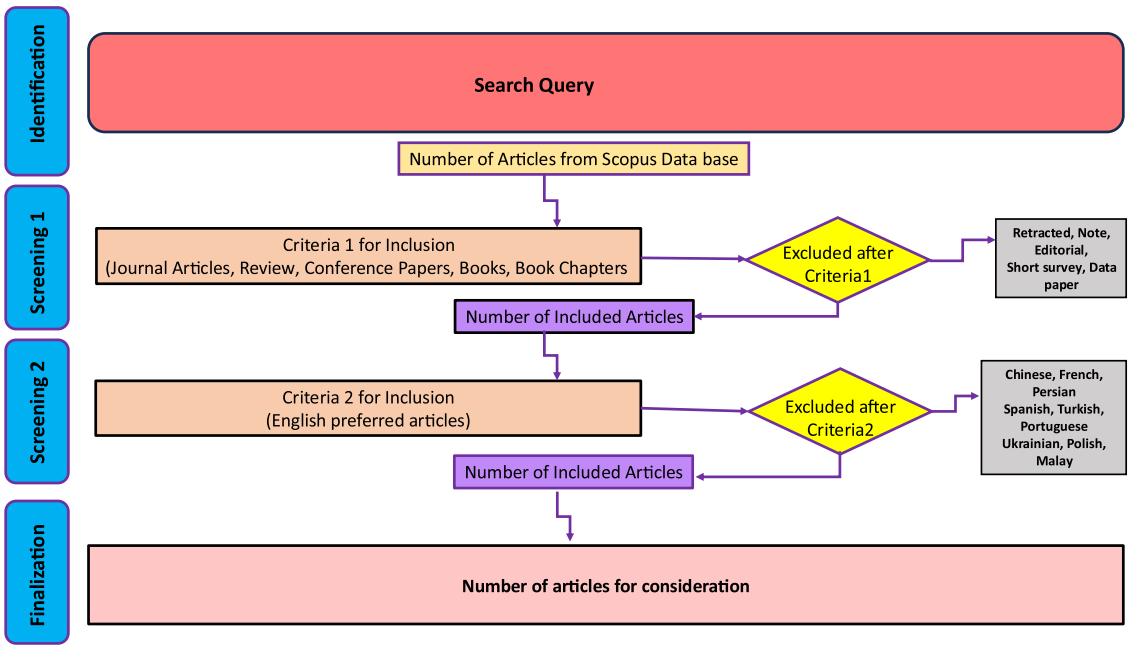

Figure 3: The PRISMA-based flowchart of the adopted methodology for articles selection and bibliometric analysis.

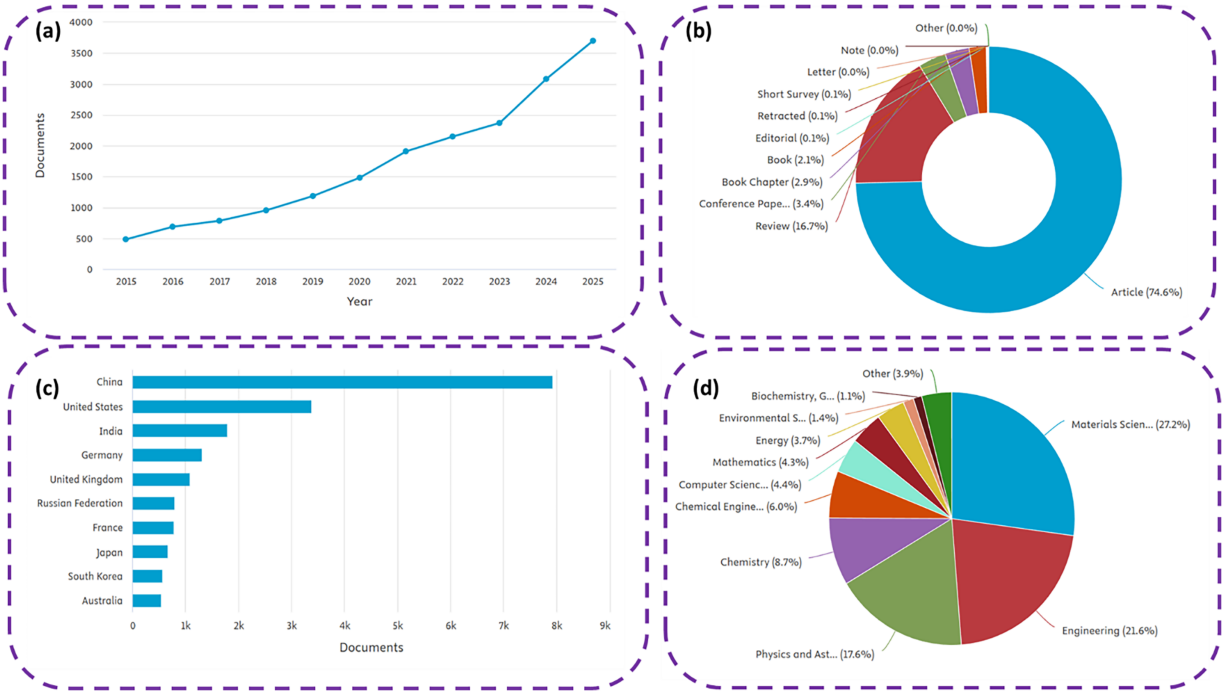

Figure 4: Bibliometric analysis of EDM-related plasma–material interaction research from the Scopus database (2015–2025).

Purely experimental and empirical studies in EDM, while valuable for capturing process trends under specific conditions, suffer from inherent limitations. Empirical models such as regression analysis and response surface methodology (RSM) are heavily dependent on the range and quality of experimental data and often lack a strong physical basis, making extrapolation to new materials, machines, or parameter spaces

unreliable. They also struggle to represent the complex, stochastic, and nonlinear interactions inherent in discharge plasma generation and material removal. Such models may fit existing data well but can fail outside the tested parameter domain, limiting their predictive capability. This challenge has been documented in recent reviews of experimental modelling techniques in EDM, which emphasise the need for physics-based and Multiphysics approaches to improve generalizability and insight into underlying mechanisms [20].

Mohd Abbas et al. (2007) highlighted that many EDM studies rely heavily on empirical experimentation and statistical correlations, which are valid only within narrowly defined process windows. They emphasised that due to the highly stochastic nature of spark discharges, empirical relationships often fail when applied to different materials, electrode geometries, or dielectric conditions. The authors noted that such approaches provide limited insight into the fundamental plasma–material interaction mechanisms, making it difficult to predict crater formation, recast layer characteristics, or energy partitioning under untested conditions [21].

Banu and Ali (2016) reviewed EDM developments and noted that most empirical studies are constrained by machine-specific settings and material-dependent constants, which limit their applicability beyond laboratory-scale experiments. They observed that empirical correlations often change significantly with slight variations in electrode material or dielectric composition, underscoring their lack of universality. The authors recommended integrating experimental work with analytical and physics-based models to overcome these limitations and improve predictive reliability [22].

Kaigude et al. (2024) investigated surface roughness prediction in EDM using machine-learning techniques and showed that classical empirical regression models underperformed advanced data-driven approaches. Their results showed that empirical models fail to capture the complex, nonlinear relationships between electrical parameters and machining responses, leading to significantly higher prediction errors. This study indirectly demonstrates the limitations of purely experimental modelling and highlights the need for hybrid approaches combining experiments with intelligent or physics-informed models [23].

Purely experimental and empirical approaches have played an important role in advancing EDM; however, their applicability remains fundamentally limited by the stochastic and highly nonlinear nature of the discharge process. Empirical models such as regression analysis, RSM, and conventional machine-learning techniques are typically developed from restricted experimental datasets and are therefore machine-, material-, and parameter-specific. As highlighted in recent reviews, these approaches often lack physical interpretability and exhibit poor extrapolation capability when applied beyond the tested domain, making them unreliable for predicting performance under new machining conditions or for advanced materials [20,24].

Complex interactions govern EDM among multiple physical phenomena, including dielectric breakdown, plasma channel evolution, Joule heating, rapid melting and vaporisation, debris transport, and solidification-driven phase transformations. These processes involve strong coupling between electrical, thermal, fluid, and materials responses, which cannot be adequately represented using single-physics or black-box empirical models. Recent studies have demonstrated that physics-based and multiphysics modelling frameworks, particularly those integrating electromagnetic–thermal–fluid domains, are essential to accurately resolve transient temperature fields, energy partitioning, crater formation, and surface integrity evolution [25].

Furthermore, the critical outcomes of EDM—such as crater morphology, recast layer thickness, residual stress distribution, and microstructural modification—arise from interactions across multiple spatial and temporal scales, ranging from nanosecond-scale plasma–material interactions at the electrode interface to macroscale heat dissipation and dielectric flow. Empirical models inherently fail to bridge these scales, leading to incomplete mechanistic understanding and inconsistent predictions. Consequently, recent studies

strongly advocate adopting multiscale modelling strategies that couple atomistic or mesoscale descriptions with continuum multiphysics simulations to capture non-equilibrium phase transformations and subsurface damage with higher fidelity [26,27].

Recent EDM research shows a clear shift from empirical parameter tuning toward integrated physics-based, data-driven, and sustainability-oriented methods. Advanced finite element analysis (FEA) and CFD are increasingly used to model plasma channel evolution, heat transfer, crater formation, and recast layer development, thereby improving predictions of MRR, surface roughness, and tool wear. In parallel, AI and machine-learning techniques (ANN, Convolutional Neural Networks (CNN), Long Short-Term Memory (LSTM), Genetic Algorithm (GA), and Particle Swarm Optimisation (PSO)) are being coupled with physical models to enable multi-objective optimisation, real-time control, and adaptive machining. Emerging trends also emphasise hybrid EDM processes (ultrasonic-, laser-, and powder-mixed EDM), micro-/nano-EDM for precision manufacturing, and green EDM using eco-friendly dielectrics and energy-efficient power supplies. Together, these trends point toward digital-twin-enabled, multiphysics, and sustainable EDM systems for next-generation manufacturing.

This review examines physics-based, multiphysics, and multiscale modelling of EDM from a computational materials science perspective, treating EDM as an extreme, localised energy–matter interaction process. The scope encompasses continuum and hybrid numerical frameworks describing dielectric breakdown, plasma channel evolution, transient heat transfer, melt pool dynamics, phase transformation, and thermo-mechanical damage, which collectively govern crater formation, recast layer development, and subsurface integrity. Advanced EDM configurations—including vibration-assisted and turning-based EDM, powder- and nano-additive-assisted EDM, and alternative dielectric media—are reviewed to elucidate how external perturbations modify boundary conditions, energy partitioning, and effective transport properties. The objectives are to critically synthesise and compare existing modelling approaches, evaluate adaptations required for advanced EDM variants, assess the role of data-driven and physics-informed AI models for rapid prediction and uncertainty reduction, and identify validation challenges, research gaps, and future directions, including pathways toward fully coupled multiscale models and digital twin-enabled predictive EDM manufacturing.

2 Fundamentals of EDM Plasma–Material Interaction

2.1 Electrical Discharge Phenomena in EDM

2.1.1 Breakdown Mechanism of Dielectric

EDM is a technique for removing electrically conducting materials by means of fast, repeated spark discharges between the tool electrode and the workpiece, in the presence of a dielectric fluid. In the EDM process, a conductive tool electrode with the specified shape is positioned near the workpiece, keeping a minimal distance referred to as the spark gap. The workpiece and electrode, particularly the spark gap region between them, are immersed in the dielectric fluid. An electrical voltage is applied between them, generating a series of sparks that lead to dielectric breakdown and significant heat, ultimately melting and evaporating materials from both the workpiece and the electrode, as illustrated in Fig. 5

2.1.2 Plasma Channel Initiation and Expansion

Fig. 6 depicts the schematic representation of the fundamental concept of the EDM process, along with the sparking and gap phenomena that occur during machining. An electric discharge occurs when a voltage is applied between the tool and the workpiece as the distance between the electrodes is reduced. Upon reaching the dielectric medium's breakdown voltage, discharge occurs, forming a plasma channel that permits current

to pass. This results in a temperature above 10,000 K, causing the material to melt and evaporate, thereby generating a rapidly growing gas bubble. Upon cessation of energy input, the plasma channel collapses, terminating the discharge. The previously generated gas bubble likewise bursts. The collapse facilitates the flow of the dielectric medium, which displaces the particles of the removed substance. The removal of material occurs through the iterative execution of this procedure, facilitated by the tool's feed in the direction of the workpiece, thereby imprinting its form into the material.

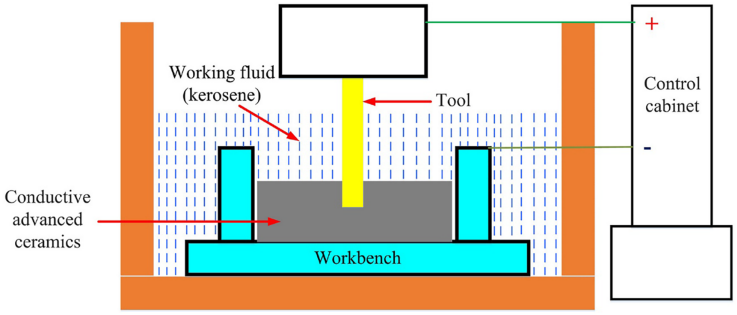

Figure 5: Basics of electric discharge machining (reprinted with permission from reference [28], 2020, Elsevier).

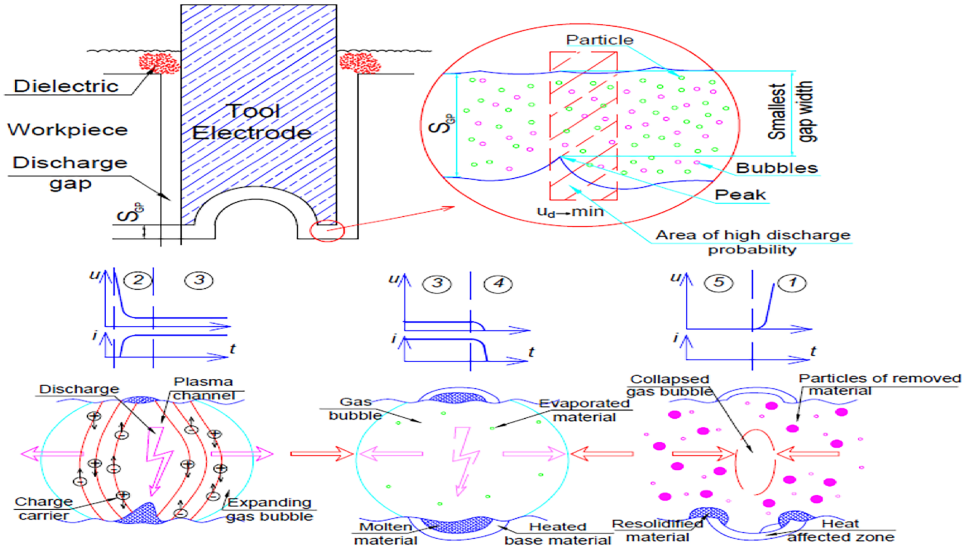

Figure 6: Plasma channel formation and material removal (reprinted with permission from reference [29], 2015, Wiley).

2.1.3 Energy Distribution between Tool, Workpiece, and Dielectric

The workpiece, tool electrode, and dielectric fluid are the three components of the closed system, where the input energy can manifest with varying intensity and duration according to the mathematical model. The energy released in the workpiece and tool electrode may be separated into three categories: conducted energy, stored energy, and energy used for the workpiece's erosion and the tool electrode's undesired wear, as shown in Fig. 7a. The dielectric fluid only distinguishes between stored and immediately transmitted energy. The remaining discharge that cannot be attributed to a specific component of the closed system manifests as many forms of energy, such as radiation, light, sound, etc [30]. The electro-thermal process, which causes material erosion at the anode and cathode due to an exceptionally high temperature driven by the high current flowing

through the plasma channel, served as the primary basis for the material-removal models. Many methods have been used to estimate the unit material removal rate of electrical discharges by predicting the electrode temperature distribution. The models may be separated into three sections: cathode erosion, anode erosion, and plasma channel according to the process characteristics, as depicted in Fig. 7b [31]. The elements of the main energy distribution are shown in Fig. 8.

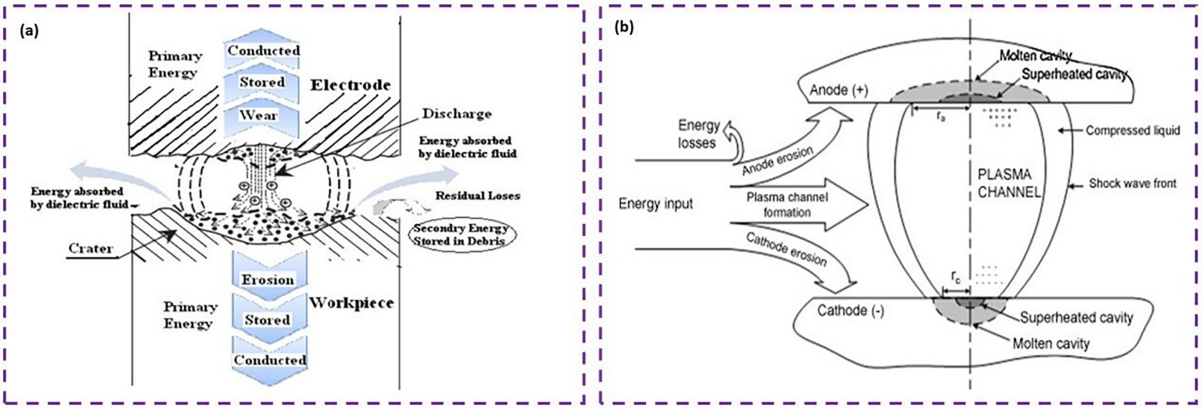

Figure 7: (**a**) Energy distribution in the EDM process (**b**) material erosion in the EDM process (reprinted with permission from reference [31], 2008, Elsevier).

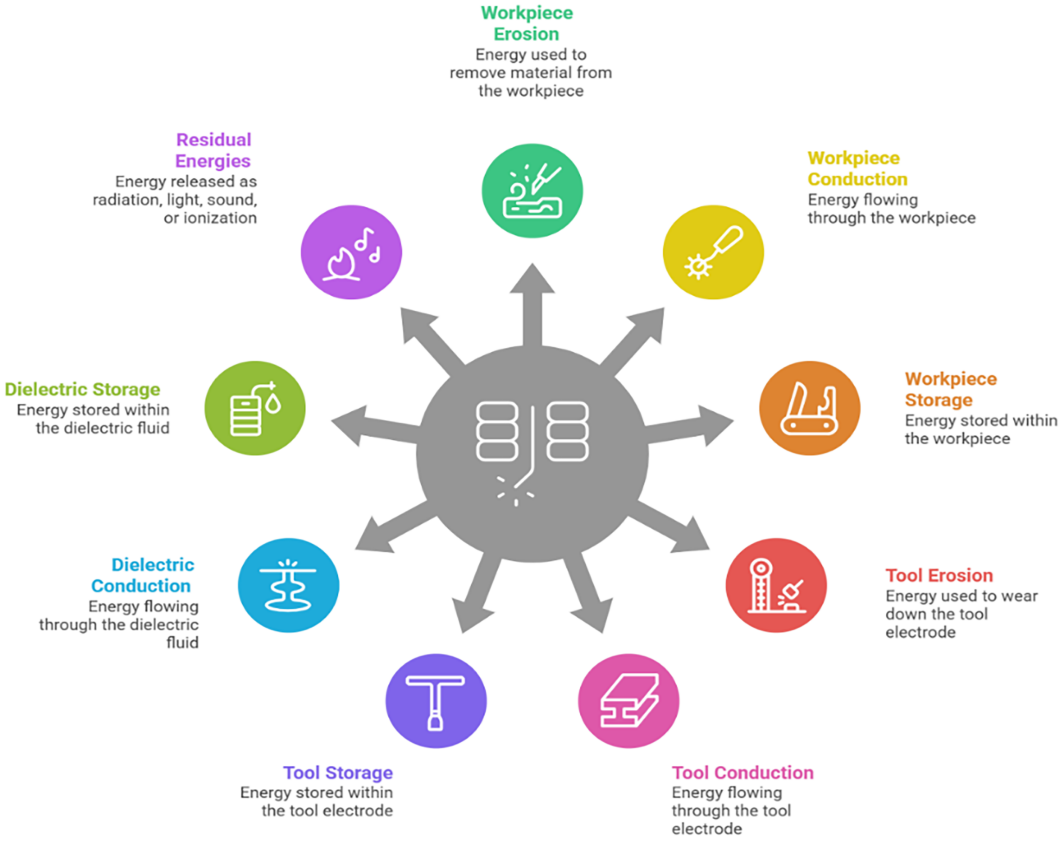

Figure 8: Primary energy distribution of the EDM process.

2.2 Time and Length Scales in EDM

2.2.1 Nanosecond-Microsecond Discharge Duration

An investigation was conducted using a thermal-fluid coupling model in COMSOL Multiphysics. The analysis focused on the influence of discharge parameters, such as peak current, pulse on-time, and the materials of the tool electrode and workpiece, on the crater formation process. Through a comparative analysis of experimental results and numerical simulations, it was observed that, at equivalent discharge energy levels, the peak current has a greater impact on the discharge crater size than the pulse on-time does. Furthermore, an analysis of the impact of tool electrode and workpiece materials revealed that crater size is affected by the boiling point of the tool electrode material and the melting point of the workpiece material. The EDM discharge parameters obtained from simulation are presented in Table 1. The electrode is composed of copper, while the workpiece is made of 65 Mn steel. With an increase in discharge peak current, there is a decrease in pulse on-time, a reduction in the high-temperature overheating area, a diminished influence range of radius temperature, an increase in discharge centre temperature, and an increase in flow rate [32].

Table 1: Conditions for simulating various combinations of discharge parameters.

Simulation No.	Peak Current (A)	Pulse on—Time (μ-s)	Discharge Radius (μ-m)	Energy Density (J/μ-m)
1	1.75	127	55.10	4.033
2	2.70	82	55.25	4.007
3	3.50	64	55.67	4.023
4	5.46	40	55.32	3.957
5	7.42	30	55.94	3.979

The numerical analysis of the plasma channel has been examined in this investigation. The illustration of the plasma channel and crater formation is shown in Fig. 9a, while Fig. 9b presents the EDM tool, workpiece, and dielectric gap, along with their configuration for simulation. The findings indicate that the plasma channel progresses through diabolo-, lantern-, and ultimately horn-shaped stages, with the diameter expansion nearly complete within 2 μs (Fig. 9c), regardless of the discharge current, upon the completion of radius expansion and shape alteration. The peak current notably influences the final dimensions of the plasma channel; however, it has minimal impact on the rules governing radius expansion, as illustrated in Fig. 9d [33].

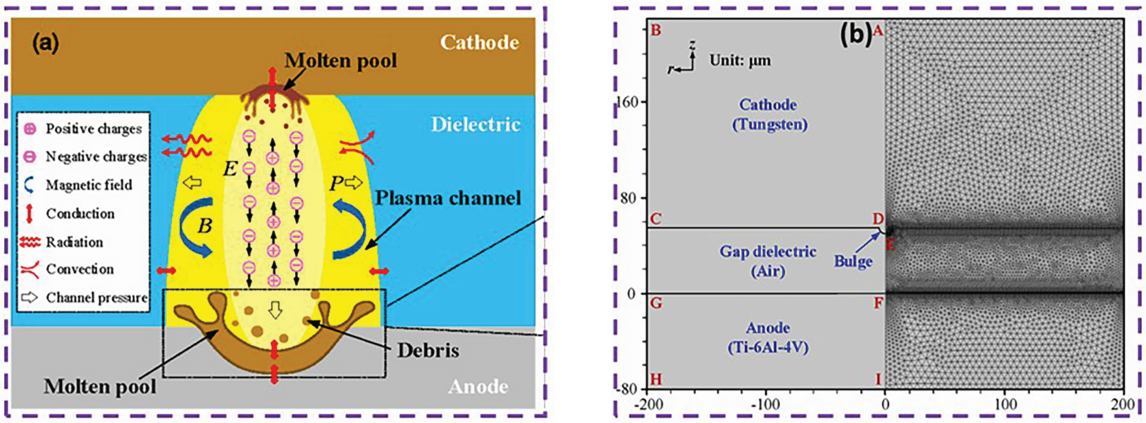

Figure 9: (Continued)

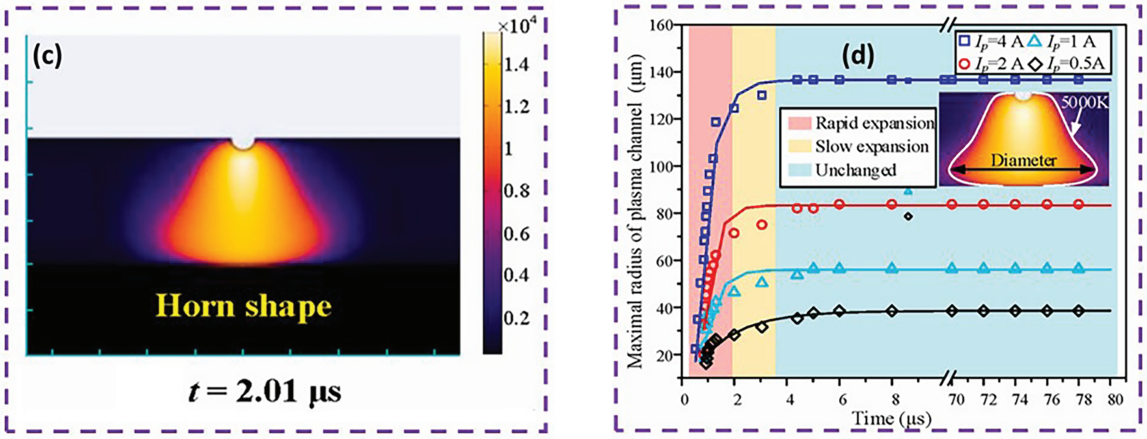

Figure 9: Numerical simulation of plasma channel, (**a**) plasma region, (**b**) tool, work piece and its meshing, (**c**) arc formation in channel, (**d**) plasma channel dimension variation with time (reprinted with permission from reference [33], 2024, Elsevier).

2.2.2 Microscale Crater Formation and Nanoscale Phase Changes

Micro/nano-EDM is an alternative technique for fabricating surface micro/nano-structures; however, precise control over their dimensions is challenging due to an ambiguous material-removal mechanism. Consequently, investigating its machining mechanism is essential to achieving efficient, controlled processing. Currently, most existing EDM thermal models for predicting discharge crater size rely on the classical Fourier heat conduction law, which assumes an infinite thermal conduction velocity. Initially, the traditional Fourier heat conduction law was amended by including a relaxation period. Secondly, many critical elements were evaluated to develop a thermal model for single-pulse micro/nano-EDM. Subsequently, numerical simulation software was used to develop the thermal model, enabling the determination of the workpiece's temperature field distribution and the prediction of discharge crater dimensions. The impact of the non-Fourier effect on the distribution of the temperature field may be described and assessed based on the findings and comparisons. Fig. 10a,b illustrates the temperature field distributions, both excluding and including the non-Fourier effect in EDM, respectively [34]. According to the comparative findings, the average thermal model inaccuracy can be reduced from 33% to 10% by accounting for the non-Fourier effect. A single pulse's shorter discharge duration makes the non-Fourier effect more noticeable. The comparative analysis of results has been presented in Table 2.

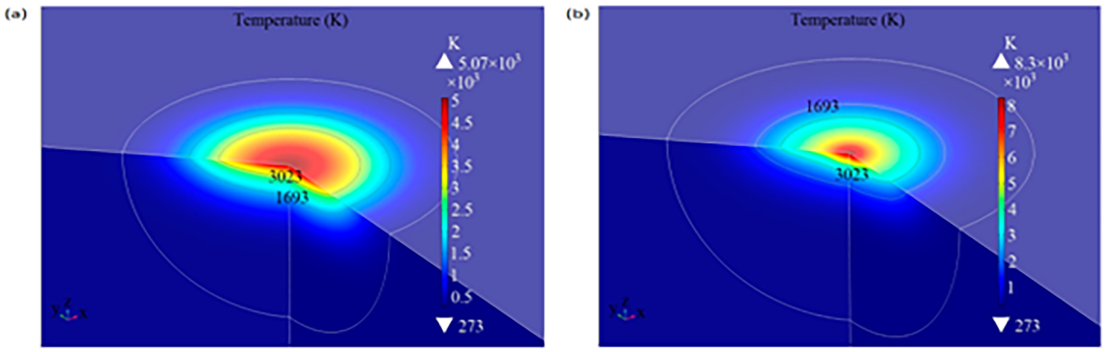

Figure 10: (**a**) Micro/nano-EDM temperature distribution without taking the non-Fourier effect into account, (**b**) micro/nano-EDM temperature distribution taking the non-Fourier effect into account.

Table 2: Numerical comparative analysis of micro/nano-EDM.

Aspect	Without Non-Fourier Effect	With Non-Fourier Effect
Maximum temperature (K)	5.07×10^3	8.3×10^3
Molten pool radius (μm)	6.0	5.63
Molten pool depth (μm)	2.03	1.87
Temperature gradient near the discharge centre	Lower	Significantly higher
Energy distribution behaviour	More uniform heat diffusion	Energy is concentrated near the discharge centre
Physical explanation	Classical Fourier heat conduction assumes instantaneous heat propagation	Heat-wave transfer delay causes transient energy accumulation at the discharge centre

In an investigation, the crater formation process was simulated using a detailed electro-thermal model of micro-EDM. Realistic machining conditions, including temperature-dependent thermal characteristics, expanding plasma radius, and Gaussian-distributed heat flux, are included in this model. This research uses commercial FEM software COMSOL. Fig. 11a illustrates the simulated workpiece temperature distribution and melting isotherm for 3300 pf, 90 V, and positive polarity machining. The melting isothermal profile is deeper within and shallower outside due to the expansion of the heat source. At the beginning, when the radius is small, energy is focused deeper inside. A lower, shallower outer surface has a shorter heating time. Fig. 11b compares computed melting isotherms to crater profiles. The simulation radius is comparable to the experiments; however, the crater depth is overestimated. This is because not all molten elements were eliminated after discharge. Unremoved molten material resolidifies and creates a recast layer following discharge [35].

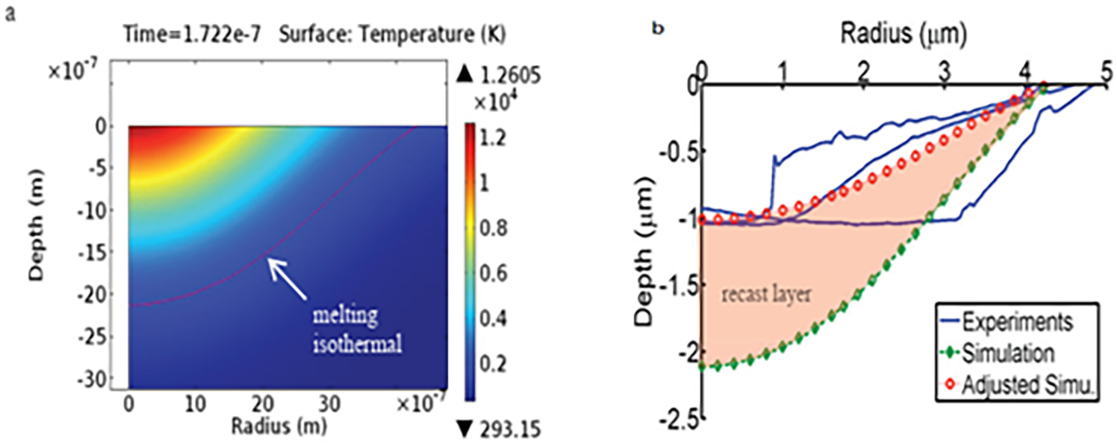

Figure 11: (**a**) Distribution of temperature of work workpiece during machining, (**b**) experimental vs. simulated results between depth of cut and radius of crater.

In a recent study, experimental and simulation analyses were conducted for the machining of carbon-fibre-reinforced ultra-high-temperature ceramic composites (C_f-UHTC) using a single-pulse EDM process. By using simulation techniques and developing a thermal–fluid coupling model, these physical variables can be thoroughly evaluated to more precisely characterise the essential physical processes during EDM, including energy conversion, transmission, and material removal mechanisms. The heat flux distribution in the plasma channel follows a Gaussian profile, with the heat source diameter on the surface matching that of the discharge channel. The plasma heat load induces phase transitions and the formation of a molten pool. The simulation findings indicate (Fig. 12a) that at low plasma energy, even though the carbon fibres are not visible at the crater's base, the bottom surface becomes uneven due to heat dissipation from the fibres. As plasma energy increases, the ceramic coating on the surface is removed, revealing the fibres beneath. Nonetheless, owing to the fibres' greater temperature resistance compared to the matrix material, their removal rate is somewhat reduced. Comparison with experimental data indicates that the simulation attains greater accuracy with an energy distribution coefficient of 0.31. Fig. 12b illustrates a contrast between the simulated and experimental data. It demonstrates that, across all processing settings, crater diameter increases with increasing spark pulse width. Fig. 12c shows that varying the plasma current enabled predicting single-pulse removal outcomes at different currents. The discharge crater diameter increases with an increase in input current [36].

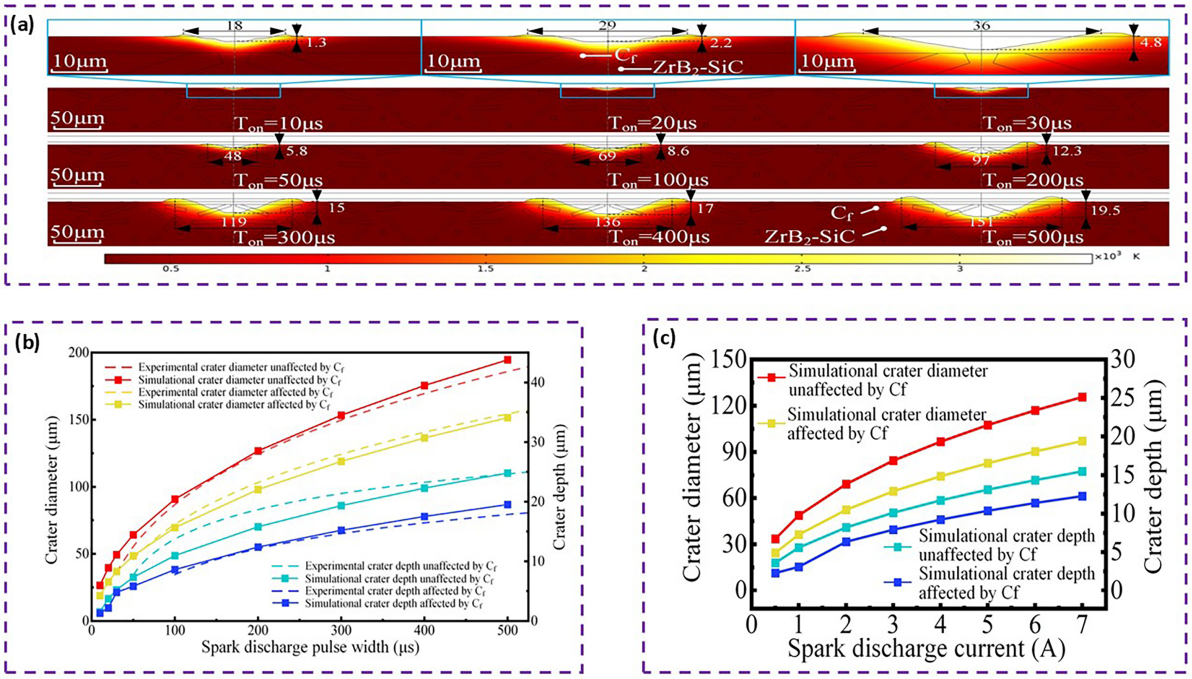

Figure 12: (**a**) Results of thermal-flow coupling simulations, (**b**) comparative analysis of variation in crater diameter with spark discharge pulse, (**c**) simulation outcomes of the discharge crater at different current levels.

2.3 Challenges of Scale Separation in Modelling

Despite substantial progress in EDM simulation, several limitations remain that necessitate careful consideration during modelling. The modelling foundation of three simulation models (FEM, MD, and flow field) is grounded in the physical phenomena of the EDM process. The use of commercial software and software packages may reduce simulation time and improve precision. The current three model types inadequately represent advanced ceramic materials, composites, and similar substances.

Given the complexity of spark processing, a single simulation model cannot solve all problems. An FEM model can determine the instantaneous temperature distribution in the discharge region [37,38]. Machining performance, including crater shape, material removal rate (MRR), surface roughness (Ra), and the recast layer, can be predicted from the temperature distribution. Nonetheless, the dynamic removal process of the material, as forecasted by the MD models, cannot be replicated using FEM models [39]. The purpose and limitations of the three model types for the EDM process are listed in Table 3.

Table 3: The purpose and disadvantages of the EDM process simulation model.

Models	Purpose	Disadvantages
FEM models.	Instantaneous temperature distribution; predicting machining performances, such as crater morphology, MRR & Ra, recast layer, etc.	Lack of research on the mechanism of material removal.
MD models.	Dynamic material removal process, machining performance prediction.	Lack of direct experimental verification; model construction is more difficult, and simulation calculation time is long.
Flow field models.	Dynamic simulation of discharge channel and flow field; prediction of machining status.	It involves multi-physical field modelling, and the model is complex; It is difficult to verify.

The computational complexity of multi-physics simulations, especially those integrating thermal, electrical, and fluid fields, poses significant challenges. These models necessitate considerable computational resources, constraining their practical use for real-time process optimisation or extensive simulations [40].

3 Governing Physics and Continuum Modelling Frameworks

The physics of EDM is governed by the coupled interaction of electric fields, transient plasma dynamics, heat transfer, and phase transformations within the workpiece material. Electrical breakdown across the inter-electrode gap leads to the formation of a highly conductive plasma channel, through which electrical energy is converted into localised thermal energy, generating extreme temperature gradients at the workpiece surface and causing rapid melting and partial vaporisation of the material [41–43]. From a continuum modelling perspective, the EDM process is described using quasi-static electric field formulations and plasma channel representations, coupled with transient heat conduction and phase change models incorporating latent heat effects and temperature-dependent material properties [44]. The plasma is commonly treated as a time-dependent thermal and pressure source, while the thermal response of the workpiece is modelled using either classical Fourier or non-Fourier heat conduction approaches, depending on discharge duration and spatial scale [45,46]. Subsequent material removal and surface modification are governed by melting, evaporation, and re-solidification mechanisms, typically represented using enthalpy-based phase transformation models [47–49]. The following subsections review plasma, thermal, and phase transformation modelling frameworks and discuss their assumptions and limitations in predicting crater formation, MRR, and surface integrity in EDM.

3.1 Plasma Channel Heat Source, Radius, and Energy Models in EDM Continuum Simulations

Continuum finite-element and finite-difference simulations of EDM almost universally reduce the discharge plasma to a prescribed, effective heat source acting on the workpiece and, in some cases, the tool electrode. Variations among published models arise primarily from differences in (i) the spatial and temporal representation of the plasma-induced heat flux, (ii) the assumed evolution of the plasma channel radius, and (iii) the partitioning of discharge energy among the workpiece, tool, and dielectric. These modelling choices strongly influence predicted temperature fields, crater geometry, MRR, and recast layer formation. The governing heat transfer differential equation can be expressed in analytical form by incorporating the effects of external heat sources [50], as given in Eq. (1).

$$\rho c_p \frac{dT}{dt} = \nabla (k \nabla T) + Q - Q_v \tag{1}$$

here, ρ is Density (kg/m^3), c_p is Specific heat (J/kg·K), k (W/m·K) denotes the thermal conductivity, T (K) represents temperature, Q (W/m^2) corresponds to the applied heat source, and Q_v accounts for heat loss due to convection.

The convective heat loss term Q_v can be expressed as follows: Eq. (2):

$$Q_v = h_c (T_s - T_0) + \varepsilon\sigma(T_s^4 - T_0^4) \tag{2}$$

here, h_c = 20 [W/m^{2}K] is the convection factor, ε = 0.09 is the emissivity, $\sigma = 5.67 \times 10^{-8}$ W/m^2·K^4 represents the Stefan–Boltzmann constant, while T_s and T_0 denote the surface and initial temperatures, respectively.

Depending on the specific validation case, the coefficients and associated factors vary, and radiative heat loss due to emission was not always included in the analysis.

3.1.1 Heat Source Representations in Continuum EDM Models

Most thermo-physical EDM models model the discharge plasma as a Gaussian surface heat flux incident on the workpiece surface, with the total power (VI) scaled by the product of discharge voltage (V) and current (I), multiplied by the fraction of workpiece energy absorption (f_w). Classical FEM investigations utilized Gaussian heat flux models incorporating latent heat considerations to estimate crater morphology and MRR. These studies showed markedly improved correlation with experimental results compared to point-source or uniformly distributed disk heat input assumptions. More recent investigations further refined this representation by explicitly relating the Gaussian standard deviation to a time-dependent plasma radius (R), represented by Eqs. (5) and (6), and scaling the heat flux magnitude with an absorbed energy fraction. f_w, showing that time-varying Gaussian sources reproduce experimentally measured crater shapes more realistically than static formulations. Comparative studies confirm that Gaussian heat flux distributions with evolving spark radius outperform point or disk sources under identical discharge energy conditions [51,52]. The Gaussian heat flux model is expressed in Eq. (3)

$$q(r) = q_0 \, exp\left\{-4.5\left(\frac{r}{R}\right)^2\right\} \tag{3}$$

Using this equation, the maximum heat flux (q_0) can be calculated using Eq. (4)

$$q_0 = \frac{4.57 f_w V I}{\pi R^2} \tag{4}$$

here, f_w is cathode energy fraction, I is discharge current (A), and V is voltage (V).

Advances in plasma-resolved simulations have enabled the calibration of more realistic heat-source profiles. Particle-in-cell Monte Carlo collision (PIC–MCC) and magnetohydrodynamic (MHD) simulations now provide time-resolved heat flux and current density fields that can be mapped directly into continuum thermal models. Qin et al. [53] demonstrated that increasing discharge current leads to a broader, flatter heat flux distribution with reduced central peak intensity, motivating the use of double-Gaussian heat source formulations in continuum crater simulations. Similar conclusions have been reported in PIC–MCC and MHD studies reveal strong temporal variation in plasma heat flux during the early microseconds of discharge evolution [54–56].

3.1.2 Plasma Channel Radius Models

The prescribed evolution of the plasma channel radius is now widely recognised as a major source of uncertainty in continuum EDM modelling [51,52]. Early and many practical FEM simulations assume a constant or semi-empirical plasma radius based on discharge current and pulse duration, simplifying implementation but failing to capture the rapid early-time expansion. It is adopted such semi-empirical current–duration-based correlations in their die-sinking EDM model, while later reviews summarised and compared similar relations across a wide range of EDM conditions [57]. Semi-empirical and time-dependent models of plasma channel radius are represented in Eqs. (5) and (6) [58].

$$R = 2040 \times 10^{-6} \times I^{0.43} \times t_{on}^{0.44} \tag{5}$$

$$R = k \times t_{on}^{0.75} \tag{6}$$

where R (m) is the plasma channel radius I (A) is current, k is a constant, and t_{on} (s) is pulse-on time.

These models fail to capture the rapid early-time plasma expansion observed experimentally, prompting the adoption of prescribed time-dependent plasma-radius laws. Shabgard et al. [59] coupled expanding plasma radii with FEM heat-transfer models to investigate plasma flushing efficiency and crater formation, demonstrating improved predictions of recast-layer thickness and material-removal trends. Papazoglou et al. [51] conducted a systematic comparison of linear, power-law, piecewise, and constant plasma radius formulations, showing that slower radial growth yields lower absorbed energy fractions but more efficient material removal, whereas faster radial growth produces narrower and deeper craters. Their comparison with experimental crater profiles suggests that power-law exponents below approximately 0.25 are most realistic [52]. Tlili et al. [60] embedded plasma channel growth and instantaneous material removal into a finite-difference framework, validating plasma radius models using measured crater geometry and MRR.

A different approach determines the plasma channel's radius by using principles from discharge physics MHD-based micro-EDM plasma models developed by Chu et al. [61] captured breakdown and expansion stages of the plasma channel, with predicted expansion behaviour confirmed experimentally. It is reported complex plasma morphology transitions during discharge evolution, while some authors [54,55] developed axisymmetric μ-EDM plasma models that accurately predicted channel diameter and temperature, achieving agreement with high-speed imaging within 5%–14.5% error. Simplified physics-based bubble models, such as those proposed by Escobar et al. [62]. Further, further provides plasma channel dimensions derived from Rayleigh-type bubble dynamics, offering an alternative route for coupling discharge physics with continuum simulations.

3.1.3 Energy Partition and Energy Fraction Models

Continuum EDM simulations require specification not only of the spatial heat flux distribution but also of the fraction of discharge energy delivered to the workpiece, the tool electrode, and the dielectric medium.

This is commonly enforced through normalised energy fractions satisfying Eq. (7).

$$f_w + f_t + f_d = 1 \tag{7}$$

where f_w, f_t and f_d represent the fractions of discharge energy delivered to the workpiece, tool, and dielectric, respectively.

These fractions are typically treated as constant or weak parameter-dependent in early models. Some experimental and analytical studies indicate that this energy partitioning varies strongly with discharge parameters, polarity, and machining scale, challenging the common assumption of constant energy fractions [57]. As mentioned by the authors [63]. The proportion of energy transferred to the workpiece typically lies between 8% and 50%.

Shabgard et al. [59] Coupled single-spark FEM simulations with experiments to derive regression relations for plasma flushing efficiency and employed these relations to predict recast layer thickness without extensive experimental testing. Gholipoor et al. [64] extended this approach by combining a new plasma radius model with FEM simulations to examine the influence of discharge current and pulse duration on plasma efficiency, showing that higher current enhances molten material ejection while longer pulse durations promote re-solidification.

More recent plasma-resolved simulations yield time-dependent energy partition factors that challenge the constant-fraction assumption. For μ-EDM, Raza and Nirala [55] demonstrated that a large fraction of discharge energy can be transported away by the dielectric, explaining discrepancies between macro- and micro-scale EDM thermal models. PIC–MCC simulations by Qin et al. [56] Further revealed a strong asymmetry in electrode energy absorption, with the anode receiving significantly more energy than the cathode under certain conditions. High-speed imaging and spectroscopy independently confirm that the plasma channel diameter, current density, and emission intensity evolve rapidly during the first few microseconds of discharge, with debris and bubble dynamics altering the effective heat flux distribution.

Overall, previous research predominantly employs radially distributed Gaussian or double-Gaussian heat source models, scaled by time-dependent energy fractions. In addition, semi-empirical and physics-based plasma radius models are widely used to capture the rapid initial expansion of the plasma channel. These approaches are further supported by energy partition formulations calibrated using plasma-scale simulations, high-speed diagnostic techniques, and continuum-based crater measurements. A comparative summary of representative plasma heat-source, radius, and energy models used in continuum EDM simulations is presented in Table 4.

Table 4: Major modelling choices across studies.

Aspect	Typical Approaches	Implications for Continuum EDM Simulation	References
Heat source shape	Single Gaussian; double Gaussian; sometimes uniform disk	Double Gaussian and time-varying Gaussians better match plasma-resolved distributions and crater shape than simple disk/point sources	[51–53,56]

(Continued)

Table 4 (continued)

Aspect	Typical Approaches	Implications for Continuum EDM Simulation	References
Radius model R	Constant; linear; power-law; piecewise; MHD/bubble-based	Strongly affects energy absorption coefficient, PFE, and crater depth/diameter; slow growth → higher removal efficiency	[51,52,59–62,64]
Energy partition	Constant f_w; regression vs. pulse parameters; plasma-resolved dynamic fractions	Controls absolute flux magnitude, micro-EDM and dry-EDM show large dielectric losses and strong anode-cathode asymmetry.	[55,56,59]

3.1.4 Assumptions and Limitations in Continuum Plasma Modelling

Continuum plasma modelling approaches employed in EDM replace the inherently discrete nature of charged particles with continuous field variables such as density, temperature, and velocity. While this approximation enables tractable numerical simulation of complex discharge phenomena, it introduces fundamental assumptions and limitations that must be carefully considered when interpreting model predictions.

A primary assumption underlying continuum and fluid plasma models is the validity of a macroscopic description. This presumes that the plasma is sufficiently collisional and spatially smooth for local thermodynamic variables and transport laws to be well defined. This assumption becomes questionable when characteristic mean free paths or relaxation times approach the scale of the inter-electrode gap, sheath regions, or early breakdown phase, where non-local and kinetic effects dominate [65]. In EDM, such conditions are frequently encountered during the ignition and extinction of individual discharges, particularly in micro-EDM and dry-EDM configurations.

To address the shortcomings of continuum and fluid plasma models in attaining non-equilibrium and non-local effects, kinetic simulation methods have been progressively studied. Particle-based methods, such as PIC methods [66], clearly resolve charged particle dynamics and collision processes, aiding accurate illustration of transient discharge behaviour, sheath formation, and non-Maxwellian energy distributions. In parallel, grid-based kinetic formulations [67] solve reduced kinetic equations in phase space, providing superior resolution of distribution functions and transport phenomena. Latest studies have confirmed the capability of such approaches to attain complex plasma dynamics beyond the scope of continuum models [68,69]. However, their high computational cost confines their direct application in full-scale EDM simulations, stimulating the development of hybrid continuum–kinetic contexts.

To reduce computational cost, many EDM plasma simulations adopt reduced dimensionality, commonly employing one-dimensional gap models or two-dimensional axisymmetric domains. These simplifications implicitly assume azimuthal symmetry and neglect stochastic discharge paths, three-dimensional tool geometry, and localised field enhancements caused by Ra or debris accumulation [54,55,70,71]. Zero-dimensional or global plasma models used in dry EDM further assume spatially uniform plasma properties, capturing only average plasma expansion and composition while sacrificing spatial resolution of heat flux and current density distributions [72].

Another major limitation arises from the treatment of plasma chemistry and species composition. Practical EDM plasma models typically include a restricted set of species and reactions to maintain numerical tractability, even though real discharge plasmas involve highly complex, transient chemistries. For example, dry EDM and micro-EDM simulations often employ reduced reaction mechanisms consisting of tens of species and several hundred reactions, which represent only a subset of the true plasma chemistry [71,72]. In low-temperature plasma fluid models, reaction networks are further pruned, which can significantly affect predicted species densities, ionisation rates, and power balance [65].

Thermodynamic assumptions also strongly influence continuum plasma predictions. Many EDM plasma models assume local thermodynamic equilibrium (LTE) or employ single-temperature formulations, thereby equating the electron and heavy-species temperatures. While TTMs partially relax this constraint, they still assume Maxwellian sub-populations and local equilibrium within each species group [70,73]. However, recent arc plasma simulations demonstrate pronounced non-LTE behaviour in EDM, particularly at low discharge currents where electron temperatures substantially exceed those of heavy species, directly violating LTE assumptions [42].

Furthermore, in the reference to non-LTE effects, EDM plasmas generated in liquid dielectrics work under very high pressures (10^7–10^9 Pa) and temperatures, where strong coupling and inter-particle interactions become important [74]. Under such conditions, the classical ideal gas assumption becomes insufficient, as it neglects Coulomb interactions, ionization-induced non-idealities, and pressure-dependent thermodynamic actions, potentially leading to large errors in predicted plasma properties. Consequently, real-gas equations of state (EOS), such as modified cubic formulations (e.g., Redlich–Kwong, Peng–Robinson) and high-accuracy polynomial or tabulated EOS, are more appropriate for describing plasma thermodynamics and dielectric–plasma transitions [75]. However, their adoption in EDM modelling remains constrained due to increased computational complexity and lack of validated high-pressure plasma data, emphasizing an important direction for increasing continuum thermo-fluid modelling accuracy.

In continuum EDM simulations, the plasma channel radius is often prescribed rather than derived from first principles. Linear, power-law, or piecewise plasma-expansion functions are commonly used to define the spatial extent of the heat source in thermal models, thereby avoiding the computational expense of full MHD plasma simulations. While these approaches capture rapid early expansion followed by stabilisation, they neglect feedback effects arising from melt pool dynamics, debris generation, and dielectric flow, which have been shown to influence plasma confinement and heat flux distribution [52,76].

In addition to bulk plasma modelling limitations, accurate representation of boundary conditions and plasma–wall interactions remain a key challenge in EDM simulations. Recent kinetic and hybrid studies have emphasized that determining energy-dependent emission processes and non-equilibrium sheath dynamics is important for improving prediction of near-surface energy transfer and discharge behaviour. Sheath behaviour, secondary electron emission, and energy-dependent surface interactions are frequently treated using simplified constants or classical sheath models, rather than fully resolved emission and reflection physics [55,77]. Recent studies highlight that implementing realistic, energy-dependent secondary electron emission within continuum kinetic frameworks is both numerically challenging and computationally expensive, leading to widespread use of oversimplified boundary treatments [65,78]. Furthermore, EDM is fundamentally a multiscale process involving tightly coupled plasma, thermal, and fluid dynamics across widely varying temporal and spatial scales. To address these challenges, advanced numerical approaches such as asymptotic-preserving schemes have been established to empower consistent solutions across regimes without deciding all microscopic scales explicitly [79]. However, the integration of such multiscale frameworks with physically accurate plasma–wall interaction models remains limited, representing an important challenge for future EDM modelling.

Beyond physical assumptions, continuum plasma models face inherent numerical and multiscale limitations. Accurate resolution of sheaths, filaments, and steep gradients requires extremely fine spatial and temporal discretisation, as well as velocity-space resolution in kinetic formulations. Such requirements are often impractical for EDM-scale simulations, necessitating grid coarsening or exclusion of near-electrode regions where non-equilibrium effects are strongest [65,70,78].

Hybrid kinetic–fluid approaches partially address this issue but rely on assumptions of locally Maxwellian distributions when coupling kinetic and fluid regions, which may fail in strongly non-equilibrium zones and compromise strict conservation properties [73].

Finally, many continuum EDM plasma models depend heavily on empirical relations. Plasma radius laws, energy fraction coefficients, and effective material properties are often tuned using crater geometry, high-speed imaging, or material removal measurements. While such a relation improves agreement within a specific operating window, predictive capability outside the calibration range—such as different dielectrics, electrode materials, or pulse regimes—remains limited. Additionally, many models neglect debris transport, bubble dynamics, turbulence, and stochastic multi-spark interactions, despite growing evidence from MHD simulations that these effects play a significant role in melt ejection, crater evolution, and surface integrity. Table 5 summarises the principal assumptions and inherent limitations of continuum plasma modelling approaches employed in EDM, highlighting the conditions under which their predictive capability may be compromised.

Table 5: Assumptions and limitations of continuum plasma modelling approaches in EDM.

Modelling Theme	Key Assumptions	Principal Limitations in EDM Context	References
Continuum (fluid) approximation	Plasma is treated as a collisional, locally smooth medium	Breaks down in sheath regions, during ignition/extinction, and when mean free paths approach gap dimensions	[63]
Dimensionality and geometry	Axisymmetric or reduced order (1D/2D/0D) discharge representation	Cannot capture stochastic discharge paths, 3D tool geometry, Ra, and debris-induced field localisation	[53,54,64,65]
Plasma chemistry representation	Reduced species set and reaction mechanisms	Partial representation of transient EDM plasma chemistry, affecting species densities and ionisation balance	[63,65]
Thermodynamic equilibrium	LTE or single/two-temperature formulations with Maxwellian populations	Non-LTE behaviour is prominent at low current and short pulse durations	[42,64,70]
Plasma channel evolution	Prescribed plasma radius or expansion laws	Ignores coupling with melt pool dynamics, debris generation, and dielectric flow	[51,55,71]
Plasma-wall interactions	Simplified sheath and secondary emission models	Uncertainty in sheath voltage, current density, and surface energy flux	[54,63,72,73]

(Continued)

Table 5 (continued)

Modelling Theme	Key Assumptions	Principal Limitations in EDM Context	References
Numerical and multiscale treatment	Coarse spatial and temporal discretization for feasibility	Under-resolution of sheaths and steep gradients; limitations near electrodes	[28,29,63,64,73]
Hybrid kinetic–fluid coupling	Local Maxwellian behaviour at kinetic-fluid interfaces	Potential inaccuracies in strongly non-equilibrium regions	[70]

3.2 Heat Transfer and Phase Transformation Models

In EDM, heat transfer and associated phase transformations govern material removal, surface integrity, and subsurface microstructural evolution. The extremely high heat fluxes and ultra-short discharge durations produce steep thermal gradients and rapid heating–cooling cycles that challenge the validity of conventional thermal assumptions. Consequently, both classical and advanced heat conduction models are required to accurately represent transient temperature fields, while robust phase transformation frameworks are necessary to capture melting, evaporation, and subsequent re-solidification of the workpiece material. This section provides a concise overview of classical and non-Fourier heat conduction formulations, modelling approaches for thermally induced phase changes, and the role of latent heat and temperature-dependent properties in realistic EDM simulations, forming a unified continuum-scale description of thermo-physical phenomena during spark erosion.

3.2.1 Classical vs. Non-Fourier Heat Conduction Models

Early and most current EDM thermal models solve the classical Fourier heat equation with conduction as the dominant mechanism, typically under single-spark, axisymmetric conditions and prescribed heat flux (point, disc, or Gaussian sources) [58,80,81]. Fourier-based models have been widely used to predict temperature fields, molten pool size, and crater geometry, and underpin many FEM and analytical formulations [82]. The classical Fourier heat equation is represented by Eq. (8).

$$q = -k \nabla T \tag{8}$$

where q is the heat flux (W/m^2), k is the thermal conductivity, and ∇T is the temperature gradient.

However, EDM involves extremely high heat fluxes (10^{11} W/m^2) and very short pulse durations (<1 μ-s in micro/nano-EDM), so the assumption of infinite heat propagation speed becomes questionable. Hyperbolic/non-Fourier formulations introduce a finite thermal wave speed via a relaxation time, leading to telegrapher-type (Cattaneo–Vernotte) equations. Analytical and numerical studies for EDM show that Fourier models can mis-predict near-surface temperatures and transient layers, and that temperature profiles can differ qualitatively under high Vernotte numbers. For micro/nano-EDM, incorporating a non-Fourier term significantly improves crater size prediction, reducing average error from 33% to 10%. The non-Fourier law proposed by Cattaneo–Vernotte has been represented as Eq. (9).

$$\tau(\partial q/\partial t) + q = -k \nabla T \tag{9}$$

where τ is the thermal relaxation time (s), accounting for finite heat propagation speed.

More general dual-phase lag (DPL) formulations and nonlocal peridynamic DPL models have been developed for transient non-Fourier heat conduction, although not always applied directly to EDM.

DPL model used [83] is represented by Eq. (10)

$$q\left(x, t+\tau_q\right) = -k \bigtriangledown T\left(x, t+\tau_T\right) \tag{10}$$

where τ_q is the phase lag of the heat flux vector, τ_T phase lag of the temperature gradient, x is space, and t is time variation during machining process.

MD with a TTM further captures electron–phonon non-equilibrium at sub-micron scales, improving representation of ultrafast heat transport in metals during EDM discharges [58,84].

3.2.2 Modelling Melting, Evaporation, Re-Solidification and Recast Layer

Most electro-thermal EDM models assume material is removed once local temperature exceeds the melting or boiling point, with the crater volume estimated from the region above these isotherms [58,80,81]. More advanced thermo-hydraulic coupling models incorporate melt pool flow, evaporation recoil pressure, surface tension and thermocapillary forces to describe molten material transport, crater shape and bulge formation. These models show that evaporation recoil pressure and Marangoni forces dominate radial melt flow and bulge formation, and that melt pool oscillations and intermittent evaporation govern debris generation and removal [85].

Surface formation and re-solidification/recast layers are increasingly treated by tracking the evolving free surface and solidification front. Arbitrary Lagrangian–Eulerian and Smoothed Particle Hydrodynamics multiphase methods simulate crater formation, overlapping of successive craters, and recast layer thickness, with good agreement to experiments [58,85]. For electrical discharge coating and hybrid arc/EDM or arc-machining of composites, transient heat transfer models including melt pool cooling, convection to the dielectric, and conduction into the substrate reproduce complex solidification microstructures, banded morphologies, and columnar grains, linking cooling rates to coating/recast layer characteristics [86,87]. While the majority of continuum EDM models utilize temperature-based criteria for phase transformation, that is, removing or melting material if (T > Tm), none of the models incorporate any explicit information about the microstructural development occurring during the resolidification stage. In order to overcome this problem, more sophisticated modelling tools, such as phase field (PF) modelling, have recently been investigated. The phase field model allows the simulation of dendrite growth, grain structure evolution, and microstructure formation inside the recast layer through diffuse interface approach without any definition of the interfaces. By incorporating the transient temperature fields simulated by means of the FEM method, the effects of rapid heating and cooling processes on the solidification process can be accounted for.

3.2.3 Latent Heat Effects and Temperature-Dependent Material Properties

A clear trend in recent EDM modelling is the explicit inclusion of latent heats and temperature-dependent thermophysical properties. Early models often assumed constant properties and ignored latent heat, leading to overpredicted crater depths and MRR [81]. Including latent heats of fusion and vaporisation increases effective thermal resistance, yielding shallower, more realistic craters and better correlation with measured MRR [51,58,80,88]. Latent heat can be implemented either as explicit phase-change energy terms or via equivalent specific heat formulations over melting and evaporation intervals, particularly in micro/nano-EDM [54,87]. The influence of latent heat associated with phase transformation on the temperature distribution in micro-/nano-EDM can be incorporated by representing it as an equivalent specific heat, as expressed in the corresponding Eqs. (11) and (12).

$$C_L = C_p + \frac{L_f}{T_m - T_r} \tag{11}$$

$$C_g = C_L + \frac{L_v}{T_b - T_m} \tag{12}$$

here, C_p denotes the specific heat of the material in the solid state, C_L represents the specific heat in the liquid state, and C_g corresponds to the specific heat in the gaseous state. L_f is the latent heat of fusion, L_v is the latent heat of vaporisation, T_r is the reference temperature, T_m is the melting temperature, and T_b is the boiling temperature of the material.

Similarly, temperature-dependent thermal conductivity, specific heat, density, emissivity, and even solid–solid phase transformations are increasingly incorporated. For difficult-to-cut alloys (Inconel 718, Ti alloys, and stainless steels) and particle-reinforced composites, accounting for property evolution with temperature and for matrix–reinforcement interfaces markedly improves predictions of temperature fields, crater geometry, and erosion efficiency. Comparative studies show that models including both latent heat and temperature-dependent properties match experimental MRR and crater metrics significantly better than simplified models [54,58,80–82,87,88]. Table 6 summarises the major EDM thermal modelling choices and their effects.

Table 6: Comparison of major EDM thermal modelling choices and their effects.

Aspect	Typical Treatment	Impact on Predictions	References
Heat conduction law	Fourier vs. hyperbolic/ non-Fourier, TTM	Non-Fourier improves ultrafast, micro/nano-EDM accuracy	[83,84]
Heat source	Point/disc vs. Gaussian, expanding plasma	Gaussian/realistic sources improve crater accuracy	[58,80–82]
Phase change	Melting only vs. melting + evaporation + re-solidification	Full treatment refines the crater volume and recasts	[54,80,81,85–87]
Latent heat	Neglected vs. fusion + vaporisation	Including latent heat reduces crater depth error	[54,58,80–82,87,88]
Material properties	Constant vs. temperature-dependent	T-dependence improves MRR and geometry prediction	[58,81,82,86,88]

4 Thermo-Fluid and Thermo-Mechanical Modelling

The EDM process combines melting and vaporisation of difficult-to-machine materials via a spark process.

4.1 Melt Pool Dynamics

The EDM melt pool consists of the dielectric and the gap between the workpiece and the tool. The dielectric in the gap ionised, and a plasma developed. The EDM model comprises three major parts: the tool, the gas, and the workpiece. In actual EDM, once the dielectric gap is broken into arc plasma, current starts flowing through the arc plasma, and a magnetic field is set up. The Lorenz force developed can deflect

the flow of dielectric, pressure, and temperature. The temperature affects the dielectric properties and the current density. Thus, the actual model involves the heat transfer analysis. The basic thermo fluid model is given in Table 7 [89].

Table 7: Thermo-mechanical modelling.

Assumptions	The dynamic analysis of the gap assumes a steady-state equilibrium arc and a monovalent dielectric that behaves as an ideal gas. The arc plasma is now considered to consist only of air and electrode material vapour, without changing the electrode materials.
Mass Conservation	$\frac{1}{r}\frac{\partial(r\rho u)}{\partial r}+\frac{\partial(\rho w)}{\partial z}=0$ where ρ is the density (kg/m^3), u is radial velocity (m/s) and w is axial velocity (m/s)
Momentum conservation equation	$\frac{1}{r}\frac{\partial(r\rho uu)}{\partial r}+\frac{\partial(\rho uw)}{\partial z}=-\frac{\partial p}{\partial r}+\frac{1}{r}\frac{\partial}{\partial r}\left(2r\eta.\frac{\partial u}{\partial r}\right)+\frac{\partial}{\partial z}\left(\eta\left(\frac{\partial w}{\partial r}+\frac{\partial u}{\partial z}\right)\right)-2\eta\frac{u}{r^2}+F_r$ $Axial: \frac{1}{r}\frac{\partial(r\rho uw)}{\partial r}+\frac{\partial(\rho ww)}{\partial z}=-\frac{\partial p}{\partial r}+\frac{\partial}{\partial z}\left(2\eta\frac{\partial w}{\partial z}\right)+\frac{1}{r}\frac{\partial}{\partial r}\left(r\eta\left(\frac{\partial w}{\partial r}+\frac{\partial u}{\partial z}\right)\right)+F_z$ where p is pressure (Pa), η is viscosity (Pa-s), F_r is radial volume force (N/m^3) F_z is axial volume force
Energy conservation	$c_p\frac{1}{r}\frac{\partial(r\rho uT)}{\partial r}+\frac{\partial(\rho wT)}{\partial z}=\frac{1}{r}\frac{\partial}{\partial r}\left(r\lambda\cdot\frac{\partial T}{\partial r}\right)+\frac{\partial}{\partial z}\left(\lambda\left(\frac{\partial T}{\partial z}\right)\right)+q_j-R$ where c_p is specific heat constant (J/kg-K), T is temperature in Kelvin, λ is thermal conductivity (W/m-K), q_j is Joules Heat (W/m^2)
Maxwell's equations	$\frac{1}{r}\frac{\partial}{\partial r}\left(r\sigma\frac{\partial V}{\partial r}\right)+\frac{\partial}{\partial z}\left(\sigma\frac{\partial V}{\partial z}\right)=0$ $j_r=-\sigma\frac{\partial V}{\partial r}$ $j_z=-\sigma\frac{\partial V}{\partial z}$ $\frac{1}{r}2\frac{\partial}{\partial r}(rB_\theta)=\mu_0.j_z$ where V is the electrical potential (V), μ_0 is the magnetic permeability of vacuum (H/m), j_r Radial component of current density (A/m^2), j_z Axial (z-direction) component of current density (A/m^2), σ Electrical conductivity of the medium (S/m) and B_θ Circumferential (azimuthal) component of magnetic flux density (Tesla, T)

Note: Mass and momentum equations are used for flow field analysis of the dielectrics; energy equations are used for heat transfer analysis; and Maxwell's equations are used for electromagnetic field analysis of the electrode, dielectric, and workpiece.*

4.2 Recoil Pressure and Vaporisation Effects

Recoil pressure and vaporisation effects play a vital role in removing material from the workpiece surface in EDM. Koyano et al. investigated the effect of thermocapillary force and evaporation recoil pressure on melt pool dynamics [90]. Thermocapillary force and evaporation recoil pressure cause the molten material to flow radially during single-pulse discharge. The simulation findings demonstrate that during arc plasma expansion, the evaporation recoil pressure decreases as heat flow drops and is progressively offset by surface tension acting on the melt pool's depression. When a material evaporates, momentum transfers between surface atoms and vaporised particles, producing the evaporation recoil pressure Eqs. (13)–(15).

$$\text{Evaporation rate} = (1-\beta_r)P_{sat}(T)\left(\frac{m}{2\pi KT}\right)^{0.5} \tag{13}$$

$$P_{recoil} = \frac{(1-\beta_r)}{2}P_{sat}(T) \tag{14}$$

$$P_{sat} = P_{atm}\exp\left[\frac{ml_v}{K}\left(\frac{1}{T_v}-\frac{1}{T_s}\right)\right] \tag{15}$$

where, β_r Recondensation (or evaporation) coefficient (dimensionless, $0 \le \beta_r \le 1$), $(1-\beta_r)$ Fraction of molecules that actually escape (evaporate), T_s and T_v surface and vapour temperature (K), respectively.

4.3 Surface Tension Driven Flow (Marangoni Convection)

The Marangoni effect describes the flow driven by a surface-tension gradient. The surface tension gradient can be created by chemical, electrical, and thermal methods. The plasma channel is assumed to have a Gaussian distribution of heat flux. This plays an important role in micro EDM. The metal liquid flows from a high-temperature region to a low-temperature region. This is dominant in the weld pool, but due to the intense temperature effect in EDM, the Marangoni effect is also seen. The molten pool is affected by hydrodynamic, buoyancy, electromagnetic, and surface-tension forces (see Table 8). The Marangoni effect was introduced to describe the shear stress at the liquid surface due to a surface tension gradient and viscosity.

Table 8: Marangoni convection surface tension.

Surface-Tension Gradient	Equations
The Marangoni convection effect is included in all three basic equations: the mass, energy, and momentum equations.	$\nabla \cdot \mu\frac{\partial}{\partial z} = \frac{\partial \gamma}{\partial T}(\nabla \mathrm{T})\frac{\partial u}{\partial z}u$, μ and γ are velocity, dynamic viscosity and surface tension, respectively.
The evaporation rate is mainly affected by the temperature and saturated vapour pressure.	$\text{Evaporation rate} = (1-\beta_r)P_{sat}(T)\left(\frac{m}{2\pi KT}\right)^{0.5}P_{sat}$ is saturated pressure, m is mass of an atom.
The effect of thermos capillary force in terms of Marangoni number [91]	$\frac{\partial \sigma}{\partial T}\mathrm{L}\frac{(T_h-T_c)}{\alpha_i u_i}\alpha_i$ is thermal diffusivity and u_i dynamic viscosity.

4.4 Crater Morphology Prediction

After dielectric breakdown, high-heat-flux plasma developed at both electrodes, leading to the melting and vaporisation of the materials. The melted materials cannot be easily removed from the spot, forming a crater. The thermo-hydraulic coupling model is used for the investigation of the discharge crater as [89]: Eqs. (16)–(18).

Mass conservation

$$\nabla \cdot u = m_s \tag{16}$$

Momentum Conservation

$$\rho\frac{\partial u}{\partial t} + \rho(u\cdot\nabla)u = \nabla\cdot\left\{-pI + \eta\left(\nabla u + (\nabla u)^T\right)\right] + F\right\} \tag{17}$$

Energy conservation

$$\rho c_p \frac{\partial T}{\partial t} + \rho c_p u \nabla T = \nabla \cdot (\lambda \nabla T) + Q \tag{18}$$

where I is the identity matrix, and η dynamic viscosity F, and λ Thermal conductivity of the material (W/m·K) is the source term used for the effect of different forces, m and Q are used for the source term used for the vaporisation of materials in the simulation. The energy conservation equation are used for flow velocity, and the pressure distribution is used for the heat transfer and fluid equations are coupled to simulate phase transitions and the flow of hot electrode materials. The equations are as follows [92]

The heat transfer and fluid equations are coupled to simulate phase transitions and the flow of hot electrode materials. The Eqs. (19)–(23) are as follows [92].

Electrode material assumes homogeneous isotropic Newtonian laminar in the liquid state. Enthalpy, thermal, and fluid properties are functions of temperature only. Property changes in the phase transition only

Momentum Conservation

$$\rho \frac{\partial u}{\partial t} + \rho \left(u \cdot \nabla\right) u = \nabla \cdot \mu \left[\nabla u + \left(\nabla u\right)^T\right] + F - \nabla \mathrm{P}\} \tag{19}$$

μ is dynamic viscosity (Pa-s), ∇P Pressure gradient force

Energy conservation

$$\rho c_p \frac{\partial T}{\partial t} + \rho c_p u \nabla T = \nabla \left(k \nabla T\right) + Q \tag{20}$$

k is thermal conductivity (w/mK)

Mass conservation

$$\frac{\partial \rho}{\partial t} + \nabla \cdot (\rho u) = 0 \tag{21}$$

The following equations can estimate the magnitude of plasma heat [93]:

$$Q\left(r\right) = Q_0 \cdot \exp\left\{-4.5 \cdot \left(\frac{r}{R_{sp}}\right)^2\right. \tag{22}$$

$$Q_0 = \frac{4.57 \cdot P_e \cdot V \cdot I}{\pi {R_{sp}}^2} \tag{23}$$

R is the radial distance from the axis of the plasma channel, Q_0 heat flux or heat input intensity (W/m^2), R_{sp} is the sparking radius at the working surface. P_e power fraction entering the electrode, V discharge voltage, I discharge current.

The evaporating pressure of the melted material can be calculated based on the temperature (evaporating). The evaporating pressure is similar to plasma pressure. The plasma pressure distribution is calculated from the Eq. (24) [94].

$$p\left(t\right) = p_0 \cdot \exp\left\{-k \cdot \left(\frac{r}{R_h}\right)^2\right. \tag{24}$$

$$p_{avg} = \frac{p_0}{2}$$

R is the distance between the heat sot the pressure point, R_h is the radius of the heat source spot, k is a constant, and P_0 is the peak or maximum pressure at the centre of the spark.

4.5 Stress, Strain, and Subsurface Damage

Open voltage has a stronger influence on thermal damage than other parameters, such as residual stress and pulse on time. Optimising the process parameters effectively controlled the depth of the thermal damage [95]. On the EDM machine surface, three damage zones are identified as the resolidified layer, the HAZ, and micro cracks. The HAZ remains a recrystallized, resolidified zone, exhibiting crystalline and amorphous zones [96].

Thermal stress can be calculated from a combination of heat transfer and structural analysis, Eq. (25) [97].

$$[d\sigma] = ([D^e] + [D^p])\mathrm{d}\varepsilon(K^{th}\mathrm{dT})\frac{\partial T}{\partial z} = \begin{cases} h\,(T - T_\infty)\ if\ R > R_{pc} \\ q\ if\ R < R_{pc} \\ 0\ for\ off\ time \end{cases} \tag{25}$$

$\sigma, \varepsilon, T, h, R_{pc}, D^e, D^p$ are stress, strain, Temperature, heat transfer coefficient, sprak radius, elastic and plastic stiffness matrix.

4.6 Crack Initiation and Residual Stress

The local in-plane residual stress profile in the subsurface of random discharge is similar, while the average in-plane residual stress shows an identical characteristic in the subsurface. The maximum residual stress is found in the subsurface rather than in the top layer. The residual stress developed high Ra. Lower discharge energy can control tensile residual stress [98].

The residual stress using the Gauss distribution model, Eq. (26) [99].

$$\sigma^*\,(\delta^*) = \frac{E\,(1-\delta^*)^2}{6S_{HS}} a_1 \exp\left(-(a_2\delta^*)^2\right)\cosh\left((a_3\delta^*\right)$$

$$x\left\{2{a_2}^2\delta + \frac{4}{1-\delta^*}\right) - a_3\tanh(a_3\delta^*)\} + \frac{E\,(3\delta^* - 2)^2}{3S_{HS}} a_1 - \frac{a_1 E\sqrt{\pi}}{a_2 12 S_{HS}} \exp\left(-\frac{a_3}{2a_2}\right)^2$$
$$\times\left\{\mathrm{erf}\left(\delta^* a_2 - \frac{a_3}{2a_2}\right) + \mathrm{erf}\left(\delta^* a_2 + \frac{a_3}{2a_2}\right)\right. \tag{26}$$

where, $\sigma*$ Effective stress, δ^* normalized strain, E elastic modulus, S_{HS} yield strength, and a_1, a_2, a_3 model constants

The transformation plastic strain rate can be calculated using Leblond's approach Eq. (27), and the phase transformation strain rate can be calculated from the microstructural images analysis [100].

$$\varepsilon_{ij} = \varepsilon_{ij}^{el} + \varepsilon_{ij}^{th} + \varepsilon_{ij}^{pt} + \varepsilon_{ij}^{tp} + \varepsilon_{ij}^{cp} \tag{27}$$

Total stain rate is sum of Individual strain rates is elastic, thermal, phase transformation, transformation plasticity, and classical plasticity.

Residual stress (σ_t) near the crater radius can be calculated, Eq. (28) [101].

$$\sigma_t = E_{ym} \times \alpha_{cte} \times (T - T_a) \tag{28}$$

$$\sigma_t = -0.0524T + 105\alpha_{cte} \tag{29}$$

$$\sigma_t = 0.00310T + 8.67E_{ym} \tag{30}$$

E_{ym}, α_{cte}, T and T_a are the modulus of elasticity, coefficient of thermal expansion, Current and ambient temperature (K), respectively.

4.7 Recast Layer and HAZ Formation

The re-solidified molten metal on the machined surface is called the recast layer. The recast layer thickness can be measured from the cross-section of the machined parts. The recast layer thickness varies from material to material [102]. The recast layer thickness can also be measured from Scanning electron microscope (SEM) images of the sample after exposure to heat near the melting point for a longer period, more than 100 h. The composition of the recast layer changes, as analysed by SEM. The HAZ developed in the EDM-machined materials due to erosion of the materials near the spark zone. The excess heat is conducted through the vicinity of the machined surface around the sparking. The HAZ lies beneath the recast layer (white layer) and forms during rapid heating and quenching cycles, leading to structural alterations, increased brittleness, and residual stresses.

Empirical relationship for recast/white layer with best fit, Eq. (31) [103].

$$Average\ Layer\ thickness = 148.5I^{0.4}t^{0.26} \tag{31}$$

White layer thickness can be measured for chrome steel, Eq. (32) [104].

$$Average\ layer\ thickness = (It)^{0.34} \tag{32}$$

where, I is peak pulse current & t pulse on time

5 Modelling of Advanced EDM Configurations

Advanced EDM configurations, including vibration-assisted EDM (VA-EDM) and turning-based EDM (EDM-T), fundamentally modify the plasma–material interaction by introducing additional kinematic degrees of freedom. From a computational materials perspective, these processes transform EDM from a quasi-static thermal problem into a fully transient, multi-physics, moving-boundary problem, requiring explicit coupling between stochastic plasma ignition, heat transfer, and phase transformation kinetics.

5.1 Vibration-Assisted and Turning-Based EDM

In both VA-EDM and EDM-T, the relative motion between the tool, workpiece, and plasma channel alters the spatial and temporal distribution of discharge energy. Consequently, modelling efforts must explicitly incorporate time-dependent heat source locations, dynamic boundary conditions, and probabilistic discharge initiation.

5.1.1 Modification of Boundary Conditions

In conventional EDM simulations, the governing transient heat conduction equation, Eq. (33) is expressed as:

$$\rho c_p \frac{\partial T}{\partial t} = \nabla \cdot (k \nabla T) + \dot{q}(x,t) \tag{33}$$

where $\dot{q}$ represents the plasma-induced volumetric or surface heat source.

For advanced EDM configurations, the heat source must be reformulated as a moving Gaussian heat flux, Eqs. (34)–(36):

$$q(x,t) = \frac{\eta V I}{\pi R^2(t)} \exp\left[-\frac{r^2(x,t)}{R^2(t)}\right] \tag{34}$$

where $r(x,t) = \| x - x_d(t) \|$ and $x_d(t)$ denotes the time-dependent discharge location.

For vibration-assisted EDM, the discharge location evolves as:

$$x_d(t) = x_0 + A\sin(2\pi f t) \tag{35}$$

while for turning-based EDM:

$$x_d(t) = \begin{bmatrix} R_w \cos(\omega t) \\ R_w \sin(\omega t) \\ z \end{bmatrix} \tag{36}$$

These formulations explicitly introduce moving thermal boundary conditions, which must be resolved numerically using adaptive time stepping as shown in Fig. 13a–c.

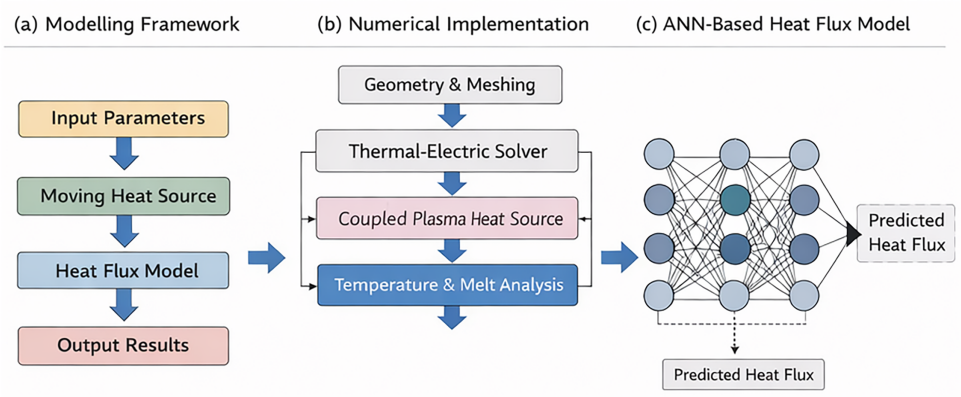

Figure 13: Computational framework for practical-assisted EDM. (**a**) Framework model, (**b**) numerical implementation, and (**c**) ANN based Heat flux model.

5.1.2 Effect on Plasma Stability and Debris Removal

Discharge initiation in EDM is inherently stochastic and governed by local gap conditions and debris concentration. Probabilistic discharge models, Eq. (37), describe the ignition likelihood as:

$$P_d(x,t) \propto \exp\left[-\frac{\tau_d(x,t)}{\tau_0}\right] \tag{37}$$

where, τ_0 is faster decay, τ_d is the local discharge delay time influenced by debris density and electric field intensity.

In vibration-assisted EDM, periodic gap modulation alters τ_d, reducing discharge clustering and promoting a more uniform spatial distribution of sparks. Computational models of massive random discharges show that this redistribution significantly reduces thermal accumulation and suppresses localized white layer thickening.

Debris transport can be approximated using an advection–diffusion formulation, Eq. (38):

$$\frac{\partial C_d}{\partial t} + \boldsymbol{u}(t) \cdot \nabla C_d = D\nabla^2 C_d \tag{38}$$

where C_d is debris concentration D is diffusion coefficient (m^2/s) and $\boldsymbol{u}(t)$ represents vibration- or rotation-induced dielectric flow velocity. Enhanced convective transport improves plasma stability and reduces arcing probability, which is depicted in Fig. 14a–c.

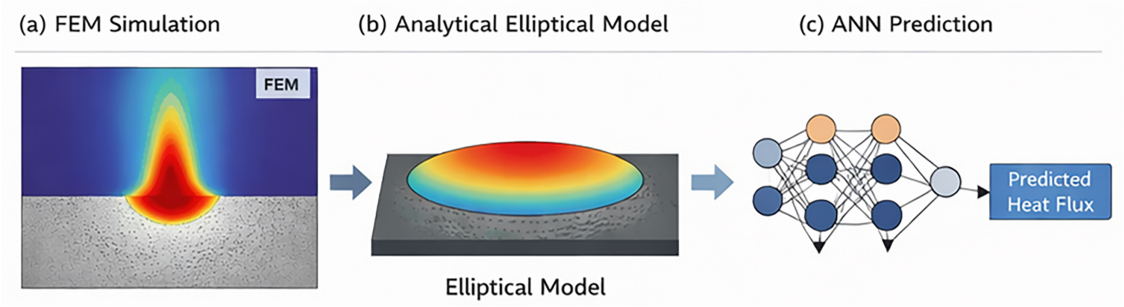

Figure 14: Predictive heat flux model in wire EDM. (**a**) FEM heat flux model, (**b**) elliptical model, and (**c**) data-driven ANN model.

5.1.3 Modelling Challenges Due to Dynamic Interfaces

The primary computational challenge in advanced EDM modelling is the treatment of dynamically evolving plasma material interfaces. Overlapping craters, moving discharge footprints, and time-dependent melting resolidification boundaries necessitate either, adaptive remeshing, element birth–death techniques, or level-set/phase-field approaches.

Material removal is typically assumed when, Eq. (39):

$$T(x,t) \geq T_m \tag{39}$$

However, advanced configurations require tracking repeated partial melting and resolidification, which directly influences microstructure evolution. T_m is the melting temperature.

Phase-field modelling, Eq. (40), of EDM-induced transformations can be expressed as:

$$\dot{\phi}_i = M\left[\sigma\nabla^2\phi_i + \Delta G_i(T)\right] \tag{40}$$

where ϕ_i is the phase-field variable, M is Phase-field mobility ($m^2/J{\cdot}s$), and $\Delta G_i(T)$ is the temperature-dependent driving force derived from the transient thermal history.

In VA-EDM and EDM-T, rapidly varying thermal gradients (10^6–10^7 K/S) combined with moving heat sources introduces strong numerical stiffness (Fig. 15a–c). Resolving plasma-scale transients, vibration frequencies, and microstructural time scales within a single simulation framework remains an open challenge in computational materials science.

5.1.4 Perspective for Computational Materials Modelling

From a computational materials standpoint, vibration-assisted and turning-based EDM demand multi-scale, multi-physics frameworks that integrate stochastic plasma models, transient heat transfer, debris

transport, and microstructure evolution. The convergence of FEM-based thermal models with probabilistic discharge mechanics and phase-field simulations represents a promising pathway toward predictive modelling of advanced EDM processes.

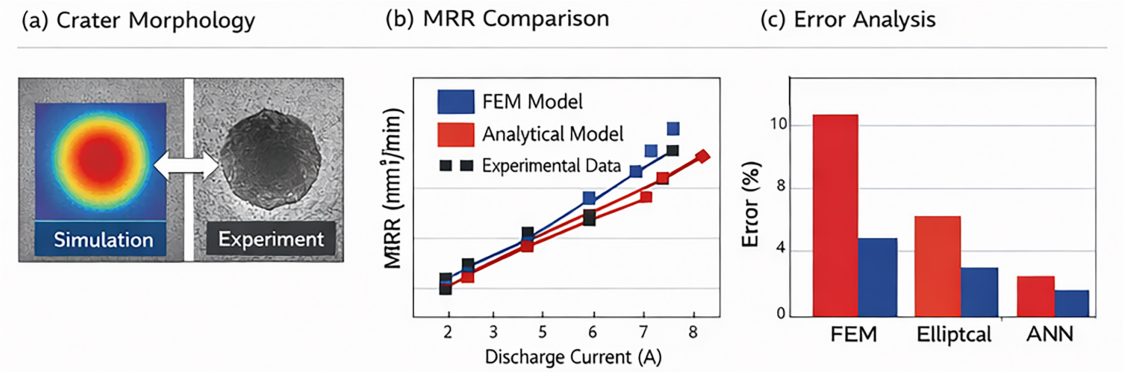

Figure 15: (**a**) Experimental and simulation, (**b**) experimental, FEM and ANN, and (**c**) error (%).

The physical interpretability and reproducibility of models can be improved by adhering to a standard computational scheme of modelling vibration-assisted or turning-aided EDM process that employs the multi-physics finite element method, whereby the discharge plasma is assumed to be a time-varying heat source, usually expressed as a time-dependent Gaussian or double Gaussian heat flux. In addition, the movement of the plasma discharge in space is handled by moving heat-source methods, whereas dynamic material interfaces are managed either by adaptive remeshing, Arbitrary Lagrangian–Eulerian (ALE), or element birth and death strategies. Typical model parameters include discharge currents within the range of 1–10 A, pulse durations varying between tens to hundreds of microseconds, and plasma channel radius of approximately 10–100 μm. Most vibration-assisted EDM modelling involves electro-thermal and thermo-fluid coupling, in which plasma effects are simplified into heat flux and pressure boundary conditions, and discharge stochasticity through probabilistic ignition models. Experimental data used in validating such models include measurements of crater profile, MRR, and thickness of recast layers obtained through high-speed camera imaging.

5.2 Powder- and Nano-Additive-Assisted EDM

Powder- and nano-additive-assisted EDM (PM-EDM and NM-EDM) introduces electrically and thermally active particles into the dielectric medium, fundamentally altering plasma initiation, energy transport, and material response. From a computational materials science perspective, these processes require explicit modelling of particle-mediated plasma modulation, effective transport properties, and coupled thermal–microstructural evolution.

5.2.1 Particle-Mediated Plasma Modulation

The presence of conductive or semi-conductive particles reduces the effective breakdown strength of the dielectric by facilitating charge accumulation and field intensification at particle surfaces, as shown in Fig. 16a–c. The discharge probability, Eq. (41) can be expressed as:

$$P_d \propto \exp\left(-\frac{E_b}{E_{\text{eff}}}\right) \tag{41}$$

where E_b is the intrinsic breakdown field of the base dielectric and E_{eff} is the particle-modified effective electric field.

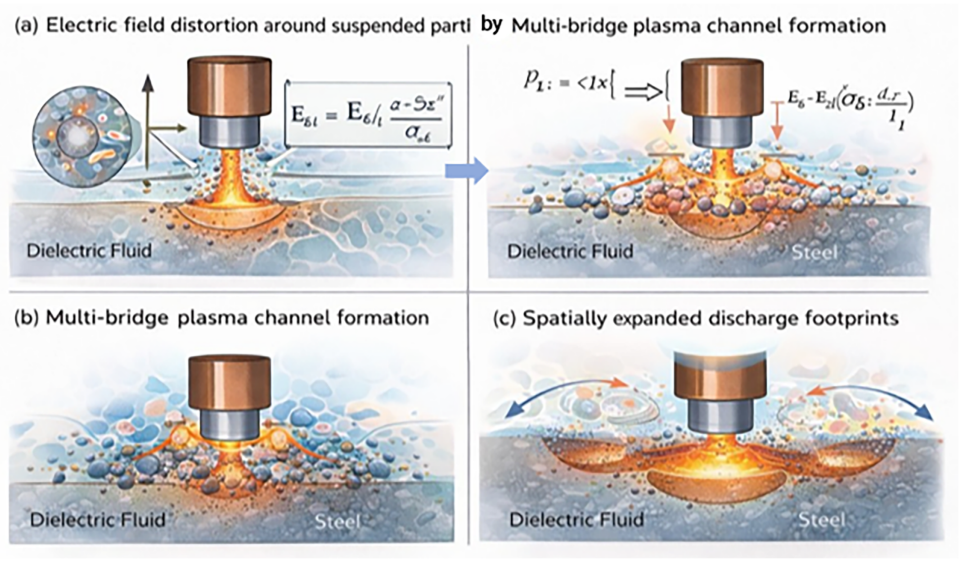

Figure 16: Practical mediated plasma modulation in PMEDM (**a**) electric field distortion by multibridge, (**b**) multibridge plasma channel, and (**c**) expanded discharge.

The local electric field enhancement, Eq. (42) around a particle of radius can be approximated as:

$$E_{\text{eff}} = E_0 \left(1 + \beta \frac{\sigma_p - \sigma_f}{\sigma_f}\right) \tag{42}$$

where, E_0, σ_p and σ_f are Young's modulus of the material, electrical conductivities of the particle and dielectric fluid, respectively, and β is a geometry-dependent enhancement factor.

Computationally, this leads to a lower discharge delay time and a broader spatial distribution of discharge sites, consistent with stochastic multi-discharge models. Particle-assisted plasma channels exhibit increased stability and reduced peak current density, which directly influences thermal loading.

5.2.2 Effective Thermal and Electrical Conductivity Models

To incorporate particle effects into FEM-based simulations, the dielectric medium is treated as an effective continuum with modified transport properties, schematic Fig. 17a,b. The effective thermal conductivity can be expressed using a Maxwell-type model Eqs. (43)–(45):

$$k_{\text{eff}} = k_f \frac{k_p + 2k_f + 2\phi(k_p - k_f)}{k_p + 2k_f - \phi(k_p - k_f)} \tag{43}$$

where ϕ is the particle volume fraction, and k_p, k_f are particle and fluid thermal conductivities, respectively.

Similarly, the effective electrical conductivity is given by:

$$\sigma_{\text{eff}} = \sigma_f \left(1 + \alpha\phi\right) \tag{44}$$

where ϕ is Internal variable, α accounts for particle chaining and percolation effects under an applied electric field.

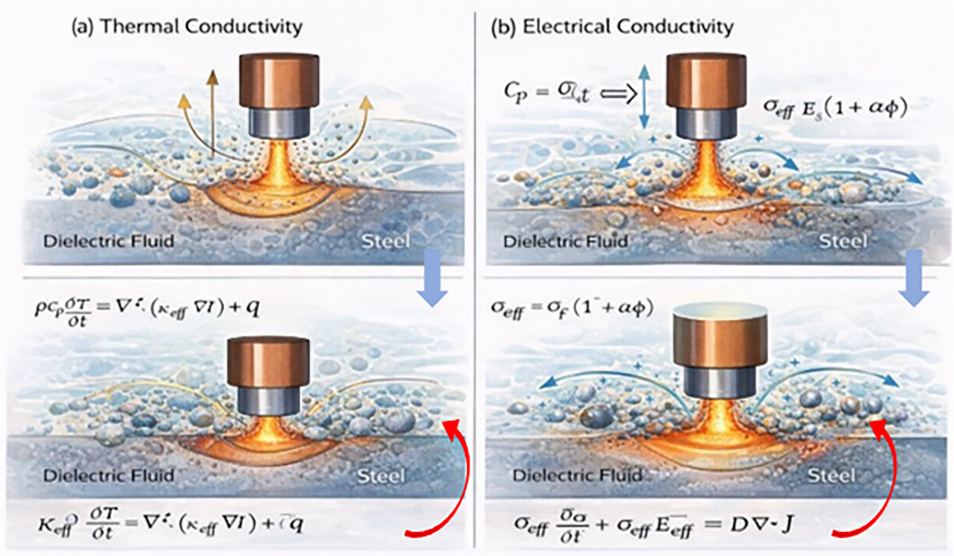

Figure 17: Effective conductive model in PMEDM. (**a**) Thermal conductivity, and (**b**) electrical conductivity.

These effective properties directly modify the governing heat equation:

$$\rho c_p \frac{\partial T}{\partial t} = \nabla \cdot (k_{\text{eff}} \nabla T) + \dot{q} \tag{45}$$

and must be coupled with stochastic discharge models to capture the spatial redistribution of energy deposition.

5.2.3 Influence on MRR and Surface Integrity

MRR in particle-assisted EDM can be estimated, Eq. (46), as:

$$\text{MRR} = \frac{60 N V_c}{T_{\text{on}} + T_{\text{off}}} \tag{46}$$

where, T_{on} is Pulse-on time (μs), T_{off} is Pulse-off time (μs), N is number of discharges, and V_c is the effective crater volume per discharge.

Particle-mediated plasma expansion increases crater diameter while reducing penetration depth, leading to higher MRR with reduced subsurface thermal damage. Multi-spark FEM simulations demonstrate that this redistribution of thermal energy suppresses excessive white-layer formation and reduces residual-stress gradients, Shown in Fig. 18a–c.

From a microstructural modelling standpoint, reduced peak temperatures and moderated cooling rates alter phase transformation pathways, particularly within the HAZ. Phase-field simulations indicate a reduction in martensitic fraction and more uniform grain refinement when particle-assisted EDM is employed.

The use of powder and nano-additive materials in the EDM process can be effectively modelled using continuum approaches combined with the effective medium theory in order to take into account the modified dielectric properties resulting from the presence of the particles. Again, the discharge plasma is assumed to act as a Gaussian heat source, but the governing equations will be modified by effective conductivities that depend on the volume fraction and particle distribution. Modelling parameters will

therefore include volume fractions, modified breakdown fields, and conductivity ratios besides the usual EDM discharge parameters like current, voltage, and pulse time. Interaction mechanisms considered during coupling will mostly include the electro-thermal and thermo-fluid phenomena where the effects of the particles are accounted for through homogenized transport properties as opposed to direct consideration of the particles. More advanced techniques may consider random multi-discharge modelling to capture discharge dispersion due to particles.

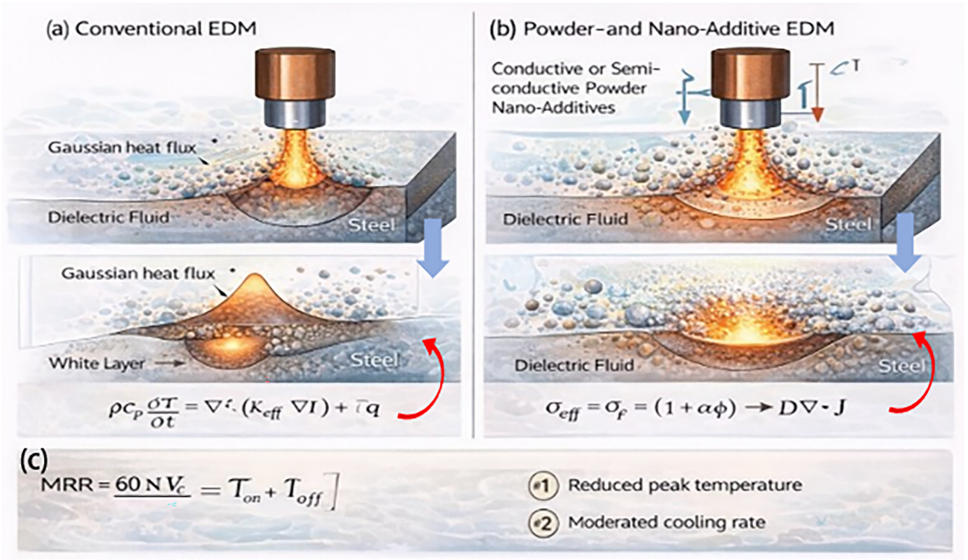

Figure 18: MRR and Ra in particle assisted EDM (**a**) conventional EDM, (**b**) powder and nano-additive EDM, and (**c**) MRR.

5.3 Alternative Dielectric Media

The choice of dielectric medium exerts a first-order influence on plasma characteristics, energy partitioning, and material response. Alternative dielectrics, including gas-based and hybrid liquid–gas systems, introduce fundamentally different plasma regimes that must be explicitly captured in computational models.

5.3.1 Gas-Based and Hybrid Dielectrics

In gas-based EDM, plasma formation occurs at reduced dielectric density, resulting in larger plasma channel radii and lower heat flux. The plasma heat flux, Eq. (47) can be expressed as:

$$q_g(r,t) = \frac{\eta_g V I}{\pi R_g^2(t)} \exp\left[-\frac{r^2}{R_g^2(t)}\right] \tag{47}$$

where η_g and $R_g(t)$ are gas-specific energy efficiency and plasma radius, respectively.

Hybrid dielectrics combine liquid flushing with localised gas injection, resulting in spatially heterogeneous plasma behaviour, in Fig. 19a–c. Computational models must therefore resolve multi-domain heat transfer while accounting for region-dependent plasma parameters.

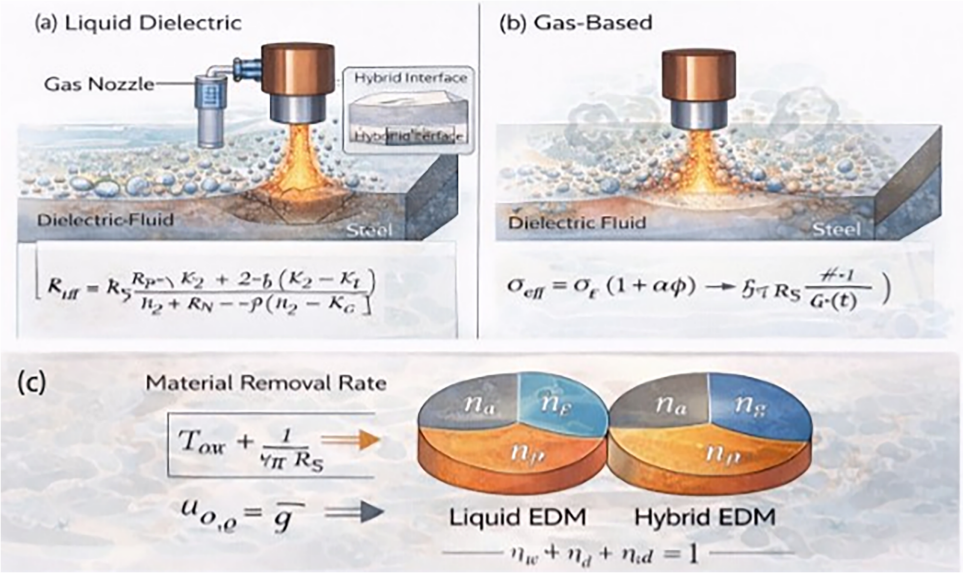

Figure 19: Gas based and hybrid dielectric EDM. (**a**) Liquid dielectric, (**b**) gas dielectric, and (**c**) MRR.

5.3.2 Energy Partitioning and Plasma Behaviour

Energy partitioning, Eq. (48), in EDM can be expressed as:

$$\eta_w + \eta_e + \eta_d = 1 \tag{48}$$

The energy partition fractions η_w, η_e, and η_d are primarily defined by the characteristics of the plasma sheath in the regions between the electrodes and the plasma sheath interface. Specifically, the energy and velocity acquired by the charged particles due to the anode fall and cathode fall voltages are key determinants of energy and momentum imparted into the anode and cathode surfaces, respectively. While electron bombardment dominates in energy imparted onto the anode, ion bombardment and secondary electron emission play a role in energy deposition on the cathode surface. The remaining energy dissipates into the plasma sheath as well as the dielectric medium through various mechanisms such as radiation and particle collisions. In summary, the energy fractions used in continuum EDM models arise as a result of the coupling between sheath voltage and particle fluxes.

Alternative dielectrics significantly alter these fractions. Gas-based EDM typically exhibits lower η_w, reducing thermal penetration depth and mitigating subsurface damage. This effect is directly reflected in FEM simulations through reduced peak temperatures and shallower thermal gradients, depicted in Fig. 20a–d. Coupling these energy partition models with phase-field simulations reveals that gas-based and hybrid dielectrics suppress extensive phase transformation while promoting finer surface morphologies.

The modelling approach generally resorts to multi-domain or heterogeneous multiphysics models to account for the specific nature of plasma behaviour in liquids, gases, or a combination of the two. In addition, the plasma heat source is modified by including dielectric-dependent energy transfer coefficients as well as plasma channel radius, leading to less intense heat flux distribution in gas dielectric. The typical values of some parameters include smaller portions of energy transfer into the workpiece as well as higher plasma channel radii in comparison with liquid dielectrics. This modelling approach relies on electro-thermal coupling with the inclusion of energy dissipation in the dielectric medium; however, fluid flow and gas phase phenomena can be included in the model through simplifying transport equations.

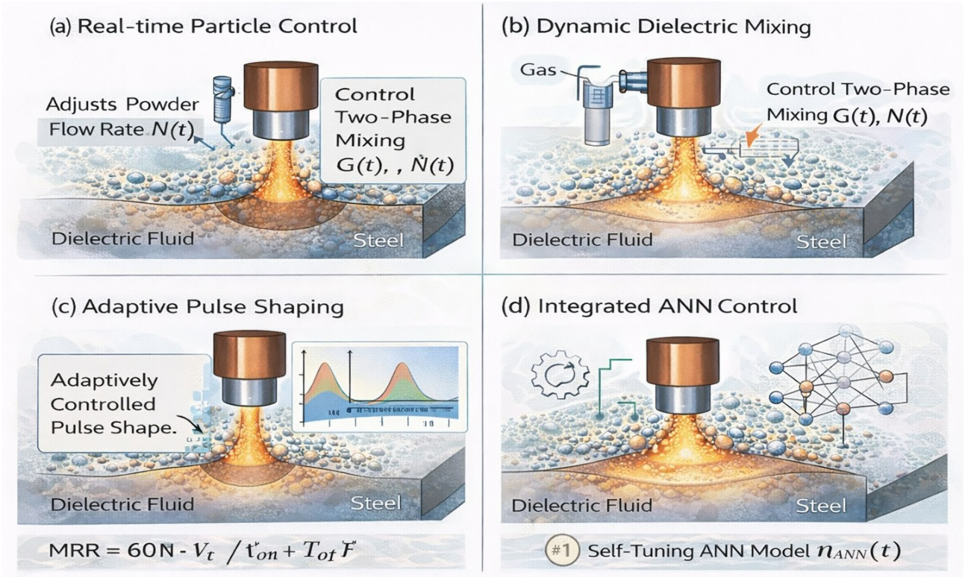

Figure 20: Hybrid EDM optimisation strategies, (**a**) real-time particle control, (**b**) dynamic dielectric mixing, (**c**) adaptive pulse shaping and (**d**) integrated ANN control.

The physics-based mathematical modeling of the EDM process employed multiple approaches to calculate crater geometry, residual stress, layer thickness, and other parameters. Most studies provide only a few analyses in a general way. The meld pool analysis is based on mass conservation, the momentum Navier-Stokes equation, energy conservation, and Maxwell equations are generally used. The details are mentioned below in Table 9.

Table 9: Multiple approaches to calculate crater geometry, residual stress and layer thickness.

EDM Process	Modelling Approach	Assumptions	Limitations	Parameters
Die-sinking EDM (macro)	Thermal FEM (Gaussian heat flux)	Axisymmetric plasma channel; constant energy fraction to workpiece	Oversimplified plasma physics; empirical energy partition	Crater diameter & depth, MRR
Wire EDM (WEDM)	Transient thermo-electric + flushing models + homogeneous isotropic Newtonian laminar	Uniform spark distribution; negligible wire vibration (basic models)	Ignores wire dynamics and stochastic discharge behavior	Kerf width, surface roughness (Ra), MRR
Micro-EDM	Multiphysics FEM (thermal + plasma + stochastic discharge)	Discrete pulse energy; size effects dominate; stochastic spark location	High computational cost; difficult experimental validation	Crater size distribution, Tool wear rate (TWR), Ra.

(Continued)

Table 9 (continued)

EDM Process	Modelling Approach	Assumptions	Limitations	Parameters
Powder-mixed EDM (PMEDM)	Modified plasma/fluid + thermal models	Altered dielectric conductivity; particle bridging effect	Complex particle interactions often simplified	Ra, white layer thickness, MRR
Dry EDM (gas dielectric)	Thermo-fluid coupled models	Gas dielectric; enhanced debris removal; reduced plasma confinement	Plasma channel assumptions less established	Recast layer thickness, MRR, tool wear
EDM of composites/MMCs	Heterogeneous material FEM + Gauss distribution model	Phase-wise thermal properties; non-uniform melting/erosion	Interface effects and anisotropy often neglected	Surface integrity, crater morphology, residual stress
Single-discharge models	Analytical/FEM thermal models	Single spark; no interaction between discharges	Not representative of real machining conditions	Single crater geometry
Multi-discharge/ stochastic EDM	Probabilistic + FEM hybrid models + Leblond's approach	Random spark location and timing	Computationally intensive; limited validation data	Surface topography, roughness, MRR
Hybrid EDM (e.g., ultrasonic-assisted)	Coupled multiphysics models	External field affects spark distribution and debris removal	Model complexity; lack of standardized validation	Simulation

6 Data-Driven and AI-Assisted Modelling in EDM

Data-driven and AI-assisted modelling have become central to understanding and optimising the highly non-linear, stochastic behaviour of EDM processes, where purely analytical models are often inadequate. Recent work spans classical statistical optimisation, soft computing, and real-time intelligent monitoring, reflecting an evolution toward smart, self-optimising EDM systems.

6.1 Statistical and Empirical Optimisation Methods

6.1.1 Response Surface Methodology (RSM)

RSM is one of the most widely adopted empirical tools for EDM and Wire-EDM, enabling the development of quadratic models that capture curvature and interaction effects among pulse parameters, current, and flushing conditions. RSM-based models have been used to describe responses such as MRR, Ra, kerf, and overcut, and to support graphical parametric sensitivity analysis and analysis of variance based significance testing. Critically, while RSM offers interpretability and modest data requirements, its polynomial structure can struggle with highly non-linear EDM behaviour and may lose accuracy near design

boundaries or under new process conditions. Some studies mitigate this by coupling RSM with optimisation methods (e.g., Non-dominated Sorting Genetic Algorithm II (NSGA-II), GRA) but still rely on relatively small, Design of experiment (DOE)-based datasets [105,106].

6.1.2 Taguchi Methods and Grey Relational Analysis (GRA)

GRA offer efficient experimental planning and multi-response optimisation. Taguchi orthogonal arrays (L9, L27) are widely used to identify influential parameters and robust settings for MRR, TWR/electrode wear rate (EWR), Ra, and kerf in die-sinking and Wire EDM. When combined with GRA, multiple objectives are aggregated into a single grey relational grade, enabling simultaneous optimisation of productivity and quality measures and yielding verified improvements in MRR and surface integrity. However, GRA requires choices in normalisation and weighting that introduce subjectivity, and the scalarization of multiple responses can mask trade-offs and response conflicts. Moreover, Taguchi–GRA frameworks are essentially off-line tools and do not inherently generalise beyond the tested design space.

The research paper has discussed about the optimization of Wire EDM process parameters (pulse-on, pulse-off, current, and bed speed) using Taguchi L16 design and ANOVA to improve accuracy, Ra, and MRR. It identifies current as the most significant factor affecting all performance measures and determines optimal parameter settings for enhanced machining performance. An Artificial Neural Network (ANN) model is developed for prediction, showing that a 70% training dataset provides the best correlation between predicted and experimental results [107].

The research paper proposed device that Nano powder-mixed EDM of Al6061 ANN and multi-objective genetic algorithms to model and optimize EWR and overcut (OC) under varying process parameters. It shows that adding alumina Nano powder with surfactant and using cryogenically treated brass electrodes significantly improves machining performance, reducing EWR and OC while enhancing dimensional accuracy. The integrated ANN–MOGA approach achieved up to ~78% reduction in EWR and 67% improvement in OC, demonstrating effective predictive modelling and optimal parameter selection for sustainable EDM [106].

6.2 Machine Learning and Hybrid Models

6.2.1 ANN

ANNs have emerged as powerful alternates for EDM and WEDM, outperforming RSM in many studies for predicting MRR, SR, kerf, wear, and sustainability metrics [106,108]. Comparative work shows ANN achieving lower prediction errors and higher R^2 than RSM for complex EDM responses, especially when interactions and non-linearities are strong. In powder-mixed and nanopowder-mixed EDM, ANN models successfully capture the coupled effects of current, pulse parameters, powder concentration, and cryogenic treatment, enabling accurate prediction of EWR, overcut, and SR and guiding multi-objective optimisation. ANN-based frameworks have also been used for bi-objective or multi-objective optimisation when integrated with evolutionary algorithms such as NSGA-II [106,109]. In a representative investigation, a multi-input, multi-output ANN was used to capture the nonlinear mapping between EDM control parameters and machining responses, enabling simultaneous prediction of kerf width, Ra, and MRR [105].

Although ANN often achieve high predictive accuracy, they operate largely as black-box models with limited interpretability and demand large, well-structured datasets along with careful regularisation strategies to mitigate the risk of overfitting [106,108,109]. Few EDM studies rigorously address model uncertainty, external validation, or transferability across different materials and machine configurations, which limits deployment in industry. The data-driven surrogate modeling approach for optimizing EDM

process parameters in machining hardened D2 steel using a Cu–SiC composite electrode, focusing on minimizing TWR and Ra. Experimental results show that discharge current, pulse on/off time, and flushing pressure significantly influence TWR and Ra, and machine learning (ML) models (Random Forest (RF), Precision-recall (PR) and Gradient Boosting (GB)) effectively predict these responses, with polynomial regression giving the highest accuracy. Finally, a firefly algorithm-based multi-objective optimization using the surrogate model identifies optimal machining parameters, improving performance while reducing experimental effort and cost [110].

The research investigated hybrid modeling approach combining Taguchi L18 design with Gaussian Process Regression (GPR) to accurately predict EDM performance parameters such as Ra, MRR, and overcut (OC). he developed GPR model effectively captures nonlinear relationships and achieves high prediction accuracy even with a small experimental dataset, validated using leave-one-out cross-validation. Multi-objective optimization based on the surrogate model identifies Pareto-optimal machining conditions, showing that graphite electrodes generally provide better performance in balancing quality and productivity [111].

6.2.2 Genetic Algorithms and Hybrid AI Frameworks

Evolutionary algorithms, particularly GA and NSGA-II, are frequently coupled with surrogate models (ANN, Adaptive Neuro-Fuzzy Inference System (ANFIS), RSM) for global and multi-objective EDM optimisation. Hybrid frameworks such as ANN–GA, ANFIS–GA, ANFIS–PSO and ANN–Multi objective genetic algorithm (MOGA) have been shown to improve prediction accuracy and yield better trade-offs among MRR, SR, TWR/EWR, energy use, and dimensional accuracy compared with single-method approaches. For gas-assisted EDM and die-sinking EDM, ANFIS–GA/PSO hybrids report lower prediction errors than standalone ANN or ANFIS, confirming the value of metaheuristic tuning of model parameters. In micro-EDM and sustainability-focused EDM, NSGA-II and MOGA are used to generate Pareto fronts that respect conflicting requirements, with confirmatory experiments validating near-optimal hole quality and surface integrity [106,109,112–114].

However, these hybrid models often entail substantial computational effort for training and optimisation, and most work remains offline. Integration with physics-based constraints remains limited; many algorithms search the design space solely from data, raising concerns about extrapolation and physical plausibility beyond the experimental envelope.

6.2.3 Real-Time Monitoring and Adaptive Control

Real-time ML-assisted monitoring and adaptive control in EDM are less mature but align with broader trends in cyber-physical manufacturing. Benchmarking frameworks such as EDM combine *in situ* PM-EDM monitoring with ML regression models, demonstrating that deep neural networks and ensemble methods can robustly predict process performance for online optimisation, thereby reducing trial-and-error and experimental costs [115]. High-accuracy ML models have also been reported for predicting electro-erosion wear and identifying dominant factors such as operating current and cryogenic treatment, with an eye toward real-time tool-condition monitoring and proactive parameter adjustment. Outside EDM, ANN-based hybrid control and adaptive recalibration frameworks in turning operations illustrate how forward and inverse neural models can support self-optimising machining and continuous updating under evolving conditions [116], offering a conceptual template for EDM.

Critically, the implementation of real-time EDM systems remains constrained by issues such as data acquisition delays, sensor reliability, limited computational capability at the machine level, and the complexity of deploying, operating, and sustaining advanced models in shop-floor conditions. There is also a lack of standardised datasets and benchmarks for streaming EDM signals, which hinders cross-study comparison and reusability of models. Summarises the comparative models and limitations of key modelling approaches are given in Table 10.

Table 10: Comparative overview and limitations of key modelling approaches.

Approach	Strengths in EDM	Main Limitations	References
RSM, regression	Interpretable, DOE-based, ANOVA, good for moderate non-linearity	Limited for strong non-linearity; local validity	[105,106]
ANN	High non-linear modelling power; better accuracy than RSM	Data-hungry; black box; overfitting risk	[105,106,108, 109]
ANFIS, ANFIS-GA/PSO	Combines rule-based interpretability with ML; improved prediction	Higher complexity; case-specific tuning	[112,113]
ANN/ANFIS + GA, NSGA-II, MOGA	Global, multi-objective optimisation with validated Pareto fronts	Computational cost, limited real-time use, weak physical constraints	[106,109,112–114]
ML-based real-time, monitoring	High predictive accuracy; potential for on-line optimization and wear prediction	Latency, deployment complexity, and lack of benchmarks	[115,116]

An adaptive EDM control system uses arcing ratio–based gap-state expectations to balance machining rate and stability, but fixed expectations can cause instability under poor chip removal or high-conductivity dielectric conditions. To address this, an extended adaptive control system is proposed with a dual-loop structure: the outer loop adjusts gap-state expectations based on machining conditions, while the inner loop controls electrode discharge timing. Experimental results show that this dual adaptive system improves robustness, stabilizes gap variations, and enhances overall machining performance. Die-sinking EDM is widely used for machining complex geometries, where spark quality significantly affects surface finish and MRR [117].

An acoustic emission (AE) signals to characterize spark activity under varying machining conditions and tool materials, showing strong correlation with process parameters and performance metrics. Incorporating AE features improves prediction accuracy of Ra and MRR, demonstrating its potential for real-time monitoring and Industry 4.0–based EDM diagnostics [118].

6.3 Impact of Dataset Shift in EDM

To understand the data shift in EDM and the research proposed hybrid technology Ensemble Learning (HEL) framework for multi-objective EDM optimization, addressing nonlinear parameter interactions and conflicting performance goals. The model, validated on 150 experiments, achieved high prediction accuracy for MRR, TWR, Ra, and overcut using advanced feature selection and uncertainty handling. Optimization

via modified NSGA-II significantly improved performance, yielding higher productivity and reduced tool wear compared to conventional methods [119].

Wire-EDM offers high precision machining but is affected by uncertainties in process parameters, which influence cutting rate and Ra. The multiple ML models to analyze noisy experimental data and identify the most accurate model for prediction and uncertainty quantification. The results shown that pulse-on time and peak current are the most sensitive parameters, providing a reliable framework for performance prediction and uncertainty analysis [120].

6.4 Strengthen the Digital Twin Section

The research proposed an integrated framework combining DOE, ANOVA, ANFIS modeling, and genetic algorithm optimization to minimize Ra during dry turning of Ti-6Al-4V. Machining parameters significantly influence cutting force, chip characteristics, and tool wear, with high prediction accuracy achieved through regression and ANFIS models.

The optimized conditions yielded minimal Ra, demonstrating the approach's effectiveness for intelligent machining and quality control [121]. The robotic EDM as a flexible solution for machining large, complex components made from hard-to-cut materials with high precision. To overcome challenges in manual control, a Digital twin (DT) of a seven-axis robotic EDM system is developed for virtual testing, collision avoidance, and kinematic optimization. The approach enables accurate gap control and user-friendly offline programming, improving efficiency and industrial feasibility of robotic EDM [122].

7 Model Validation and Experimental Correlation

Robust validation of physics-based EDM models requires systematic correlation between numerical predictions and experimentally measurable quantities. Given the inaccessibility of plasma-scale variables, validation efforts rely on indirect diagnostics, post-process surface characterisation, and statistically interpreted experimental data. Experimental findings highlight the significant role of data in improving the accuracy and reliability of EDM simulation models through calibration and validation.

7.1 Challenges in Measuring Plasma Temperature and Pressure

Direct experimental measurement of plasma temperature and pressure in EDM remains infeasible due to the ultra-short discharge duration (microseconds), micron-scale plasma channel dimensions, and optical obstruction by the dielectric medium. Consequently, experimental validation of plasma models relies on electrical pulse diagnostics and inferred thermodynamic states.

High-speed acquisition of voltage–current waveforms in Wire-EDM provides experimentally measured pulse energy distributions, ignition delay times, and discharge classifications (normal, arcing, short-circuit). Experimental studies show that stable machining corresponds to a narrow, unimodal pulse energy distribution, while instability and impending wire breakage are preceded by energy distribution leakage and increased abnormal pulse ratios [123]. These experimentally observed transitions are frequently used to validate stochastic plasma initiation and discharge probability models.

Numerical models typically back-calculate plasma temperature and pressure by matching simulated heat flux magnitudes to experimentally observed pulse energies. However, this indirect validation introduces uncertainty, as multiple combinations of plasma radius, temperature, and pressure can reproduce similar electrical signatures. As a result, plasma parameters in simulations should be interpreted as effective quantities rather than directly measurable physical states.

7.2 Validation of Crater Geometry and Recast Layer Thickness

Crater geometry remains the most widely used experimental benchmark for validating EDM simulations. Experimental crater diameter, depth, and volume are routinely measured using optical profilometry, SEM, and confocal microscopy. Studies consistently demonstrate that single-discharge crater dimensions scale with pulse energy and discharge duration, validating Gaussian or elliptic heat flux formulations adopted in FEM models.

However, experimental evidence from multi-pulse and continuous machining conditions shows that crater overlap and partial remelting dominate surface evolution, rather than isolated crater formation. Multi-discharge and massive random discharge models reproduce experimentally observed surface morphologies more accurately than single-spark simulations by accounting for spatial discharge clustering and thermal accumulation effects [124].

Recast (white) layer thickness is experimentally validated through cross-sectional SEM analysis and metallographic etching. Experimental data indicate that recast layer thickness varies not only with discharge energy but also with dielectric type, flushing efficiency, and workpiece material. In advanced materials such as ultra-high-temperature ceramics and ceramic matrix composites, experiments reveal non-uniform recast layers with microcracks, porosity, and compositional gradients [125].

Numerical thermal models often predict recast layer depth based on peak temperature contours exceeding melting temperature. While this approach captures trends, it frequently overestimates recast thickness because it neglects melt expulsion, vapor-driven ejection, and non-equilibrium solidification kinetics observed experimentally.

7.3 Correlation with Experimental Process Data and Data-Driven Validation

Beyond geometric validation, experimental process data such as MRR, Ra, and tool wear ratio provide additional constraints for model validation. Experimental studies demonstrate strong correlations between discharge energy, pulse parameters, and MRR across both metallic and ceramic materials.

In cases where physics-based models struggle to capture nonlinear interactions, data-driven and hybrid validation approaches have proven effective. ANN models trained on experimental EDM datasets consistently outperform linear regression in predicting Ra and complex material responses, particularly for advanced materials with temperature-dependent properties [125]. These models are frequently used to validate or correct FEM predictions by identifying systematic deviations between simulations and experiments.

Experimental pulse-train analysis further highlights discrepancies between assumed constant energy partitioning in simulations and the highly variable energy distribution observed in practice. This variability explains why simulations may match average MRR yet fail to reproduce transient surface damage or instability onset seen experimentally.

7.4 Inconsistencies between Simulations and Experiments

Despite qualitative agreement, quantitative inconsistencies persist due to several experimentally confirmed factors. First, energy partitioning is not constant; experiments show that the fraction of energy transferred to the workpiece fluctuates with debris concentration, discharge mode, and dielectric breakdown state. Fixed partition coefficients used in simulations therefore introduce systematic error.

Second, experimental measurements themselves exhibit scatter. Crater dimensions, recast layer thickness, and Ra show significant variability even under nominally identical conditions due to stochastic discharge behaviour and debris-mediated secondary discharges. Such variability is reflected in experimental datasets used for ANN and statistical modelling, underscoring the probabilistic nature of EDM processes.

Finally, there exists a scale mismatch between continuum thermal models and plasma-scale physics. High-fidelity CFD and combustion modelling studies demonstrate that turbulence–reaction interactions and stochastic mixing strongly influence energy localization. Similar effects are expected in EDM plasma channels but are rarely resolved explicitly, contributing to discrepancies between simulations and experiments.

8 Current Challenges and Research Gaps

Recent advances in EDM research increasingly demonstrate that purely empirical and single-physics models are inadequate for capturing the highly transient and nonlinear plasma–material interactions that govern material removal, surface integrity, and subsurface phase transformations. Traditional regression- or data-fitting-based approaches often provide acceptable predictions only within narrow experimental windows and fail to extrapolate across different materials, discharge energies, or dielectric conditions. As EDM involves tightly coupled electrical-discharge phenomena, rapid heat transfer, melt–vapour dynamics, and solidification-driven microstructural evolution, recent reviews emphasise the need for physics-based frameworks that can represent these interacting mechanisms with greater physical fidelity.

In this context, shown in Fig. 21, Ulhakim et al. (2025) highlight significant progress in integrating finite element–based multiphysics simulations with AI to enhance predictive accuracy and enable real-time process control. Their review identifies critical gaps in conventional modelling approaches, particularly in describing energy partitioning, plasma channel evolution, and thermo-fluid interactions [126]. Complementing this perspective, Yu et al. (2025) systematically analyses flow-field and multiphysics coupling models that integrate electric, thermal, and fluid domains, demonstrating how dielectric flow, bubble dynamics, and debris transport significantly influence discharge stability and crater formation. These studies collectively underscore that accurate prediction of EDM outcomes requires fully coupled multiphysics representations rather than isolated domain analyses [40].

Figure 21: Current challenges in physics-based, multiphysics and multiscale modelling of EDM.

Beyond multiphysics coupling, recent research also addresses the challenge of multiscale bridging and experimental validation. Alshaer et al. (2024) demonstrate the potential of particle-based methods, such as

smoothed particle hydrodynamics, to bridge continuum-scale thermal modelling with microscale melt flow and material ejection, offering improved insight into crater morphology and recast layer formation [58]. Meanwhile, experimental–simulation investigations by Su et al. (2024) emphasize the importance of accurate plasma characterization for validating numerical models, particularly under multi-channel and high-energy discharge conditions [127]. Finally, hybrid approaches that merge physics-based models with data-driven techniques, as proposed by Cheng et al. (2023), represent a promising pathway toward physics-informed ML frameworks, capable of overcoming data scarcity while preserving physical consistency. Together, these advances point toward an emerging paradigm of multiphysics, multiscale, and AI-assisted modelling as essential for next-generation predictive EDM research [128].

9 Future Perspective of Digital Twin Technology

The future development of DT technology is expected to be driven by the convergence of multi-physics modelling, multiscale simulation, real-time data integration, and AI, enabling a transition from descriptive digital representations to fully autonomous, predictive cyber–physical systems. In manufacturing-centric applications such as EDM and advanced forming processes, DTs will increasingly incorporate fully coupled thermal–electrical–fluid–plasma models, allowing accurate prediction of process stability, debris dynamics, material removal mechanisms, and surface integrity under dynamically changing conditions [129]. A major future direction involves integrating multiscale modelling frameworks with digital twin architectures. As highlighted by advances in multiscale and multiphysics simulations, next-generation DTs will seamlessly link atomistic, mesoscopic, and continuum-scale phenomena to macro-level process outcomes. This capability is particularly critical for accurately capturing microstructural evolution, tool–workpiece interactions, and defect initiation mechanisms, which remain inadequately represented in conventional single-scale twins. The integration of high-performance computing with scalable DT platforms will further support such hierarchical and concurrent multiscale implementations [130,131]. The role of AI and ML in future DT systems will expand from data analytics to physics-aware intelligence, in which AI models are embedded within simulation loops to accelerate computation, reduce model uncertainty, and enable real-time adaptability. Hybrid AI–FEM and physics-informed learning approaches are expected to significantly reduce computational cost while maintaining physical interpretability, making real-time DT deployment feasible for complex dynamic systems and smart manufacturing environments. This paradigm shift will be essential for achieving intelligent DTs capable of continuous self-learning and evolution [132]. Another critical perspective is the evolution of DTs from passive monitoring tools to closed-loop predictive and prescriptive systems. Future DTs will not only forecast system behaviour but will autonomously recommend or execute corrective actions through tight integration with sensors, actuators, and control systems. Such capabilities are particularly relevant for additive manufacturing, machining, and transportation infrastructure, where DTs can enable proactive defect mitigation, adaptive maintenance scheduling, and lifecycle-wide performance optimization [133].

Interoperability and integration across digital ecosystems will also shape the next phase of DT research. The relationship among DTs, building information modelling (BIM), and digital threads will become more standardised, enabling unified data flow across the design, manufacturing, operation, and decommissioning stages. This integration is crucial for achieving full-lifecycle DT implementations in large-scale infrastructure and industrial systems, reducing data redundancy and improving decision coherence. Despite rapid progress, several challenges must be addressed to realise next-generation digital twins, including heterogeneous data management, real-time synchronisation, model validation, explainability of AI-driven predictions, and the lack of universal standards. Addressing these issues will require interdisciplinary research combining physics-based modelling, data science, and systems engineering. Future efforts toward standardised DT

architectures, interpretable AI models, and secure data governance frameworks will be essential to establish digital twins as a foundational technology for Industry 5.0 and intelligent engineering systems.

10 Conclusion

This review has presented a comprehensive synthesis of physics-based, multiphysics, and multiscale modelling approaches for EDM from a computational materials science perspective. By consolidating plasma physics, transient heat transfer, thermo-fluid flow, phase transformation, and thermo-mechanical damage models, the study establishes EDM as a prototypical extreme-energy matter-interaction problem that requires a tightly coupled numerical treatment across spatial and temporal scales.

The analysis demonstrates that conventional single-physics and empirical frameworks are insufficient to capture the inherently stochastic, nonlinear, and multi-domain behaviour of EDM. Continuum plasma models based on Gaussian or double-Gaussian heat sources, time-dependent plasma radius formulations, and energy partition coefficients provide reasonable crater-scale predictions when carefully calibrated. However, experimental evidence shows that plasma temperature, pressure, and energy fractions are strongly time-dependent and influenced by dielectric composition, debris concentration, and discharge regime. Consequently, constant energy-partition assumptions and static heat-source representations introduce systematic modelling uncertainty. Advanced thermal formulations incorporating non-Fourier heat conduction, latent heat of fusion and vaporisation, and temperature-dependent material properties significantly improve predictive fidelity, particularly in micro-/nano-EDM regimes where ultrafast heating invalidates classical Fourier assumptions. Coupled thermo-hydraulic models further reveal that evaporation recoil pressure, Marangoni convection, and plasma pressure govern melt ejection and crater morphology. Nevertheless, discrepancies between simulated and experimental crater depths and recast layer thickness persist due to incomplete representation of melt expulsion, multi-spark interactions, and dielectric–plasma feedback mechanisms.

For advanced EDM configurations such as vibration-assisted, turning-based, powder-mixed, nano-additive, gas-based, and hybrid dielectric systems—the modelling challenge intensifies. These processes introduce dynamic boundary conditions, moving heat sources, modified electric-field distributions, and altered transport properties. Effective medium formulations and stochastic discharge models offer tractable representations; however, rigorous coupling between plasma evolution, dielectric flow, and microstructural phase transformation remains an open research frontier.

The review also highlights the increasing integration of data-driven and AI-assisted modelling. ANN, ANFIS–GA hybrids, and multi-objective optimisation frameworks have demonstrated superior predictive accuracy for MRR, Ra, and tool wear compared with traditional regression approaches. Yet, most AI models remain black-box predictors with limited physical interpretability and weak extrapolation capability. Emerging physics-informed ML and hybrid simulation–AI frameworks represent a promising pathway toward uncertainty-aware and computationally efficient predictive systems. From a validation standpoint, crater geometry, recast layer thickness, residual stress distribution, and pulse-energy statistics remain the primary measurable benchmarks. However, plasma-scale variables remain experimentally inaccessible, requiring indirect inference through electrical diagnostics and inverse modelling. The stochastic nature of discharge events and the variability observed in experimental datasets underline the necessity of probabilistic modelling frameworks rather than deterministic single-spark assumptions.

Acknowledgement: The authors gratefully acknowledge the support and facilities provided by the Center for Alternative and Renewable Energy and the Department of Mechanical Engineering, Rajkiya Engineering College, Azamgarh, for carrying out some portion of the present study. The author also acknowledges the use of image processing software and AI tools (OpenAI's ChatGPT) to enhance the manuscript.

Funding Statement: The authors received no specific funding for this study.

Author Contributions: All authors contributed to the study conception and design. Data collection and analysis were performed by Kamlesh Paswan, Chandrmani Yadav, Rajnish Singh, Vivekanand Singh, Brihaspati Singh and Ankur Saxena. The first draft of the manuscript was written by Kamlesh Paswan and Chandrmani Yadav. All authors commented on previous versions of the manuscript. All authors reviewed and approved the final version of the manuscript.

Availability of Data and Materials: The authors confirm that the data used to support the findings of this study are available within the manuscript. The raw data that support the findings of this study are also available from the corresponding author upon request.

Ethics Approval: This study did not involve human participants, animal subjects, or personal data. Therefore, ethical approval was not required in accordance with institutional and journal guidelines.

Conflicts of Interest: The authors declare no conflicts of interest.

References

1. Bayki S, Mujumdar S. A 1D model for prediction of dry electrical discharge machining (dry-EDM) plasma characteristics. J Manuf Process. 2023;102(4):417–28. doi:10.1016/j.jmapro.2023.07.036.
2. Wiessner M, Hollenstein C, Wegener K. Investigation on EDM plasmas using time and spatially-resolved optical emission spectroscopy. Procedia CIRP. 2020;95:183–8. doi:10.1016/j.procir.2020.02.303.
3. Ho KH, Newman ST. State of the art electrical discharge machining (EDM). Int J Mach Tools Manuf. 2003;43(13):1287–300. doi:10.1016/S0890-6955(03)00162-7.
4. Klocke F, Schneider S, Mohammadnejad M, Hensgen L, Klink A. Inverse simulation of heat source in electrical discharge machining (EDM). Procedia CIRP. 2017;58:1–6. doi:10.1016/j.procir.2017.03.178.
5. Abu Qudeiri JE, Zaiout A, Mourad AI, Abidi MH, Elkaseer A. Principles and characteristics of different EDM processes in machining tool and die steels. Appl Sci. 2020;10(6):2082. doi:10.3390/app10062082.
6. Zhang Z, Zhang Y, Ming W, Zhang Y, Cao C, Zhang G. A review on magnetic field assisted electrical discharge machining. J Manuf Process. 2021;64(13):694–722. doi:10.1016/j.jmapro.2021.01.054.
7. Rahman MA, Saleh T, Jahan MP, McGarry C, Chaudhari A, Huang R, et al. Review of intelligence for additive and subtractive manufacturing: current status and future prospects. Micromachines. 2023;14(3):508. doi:10.3390/mi14030508.
8. Li M, Yang Z, Dong H, Zhou Y, Liu Y. Machining performance of high energy die-sinking electrical discharge machining on GH2132. Mater Manuf Process. 2020;35(9):1024–31. doi:10.1080/10426914.2020.1758328.
9. Abbas JK, Aghdeab SH, Al-Habaibeh A. Investigating the effect of process parameters on surface roughness of AISI M2 steel in EDM using deep learning neural networks. Int J Adv Manuf Technol. 2025;137(1):251–62. doi:10.1007/s00170-025-15184-9.
10. Cetin A, Atali G, Erden C, Ozkan SS. Assessing the performance of state-of-the-art machine learning algorithms for predicting electro-erosion wear in cryogenic treated electrodes of mold steels. Adv Eng Inform. 2024;61:102468. doi:10.1016/j.aei.2024.102468.
11. Li L, Sun S, Xing W, Zhang Y, Wu Y, Xu Y, et al. Progress in simulation modeling based on the finite element method for electrical discharge machining. Metals. 2024;14(1):14. doi:10.3390/met14010014.
12. Ye L, Qian J, Reynaerts D. A physics-informed CNN-TSE hybrid network for micro-EDM process monitoring and control. Mech Syst Signal Process. 2023;202(2):110685. doi:10.1016/j.ymssp.2023.110685.
13. Wiessner M, Macedo FTB, Martendal CP, Kuster F, Wegener K. Fundamental investigation of EDM plasmas, part I: a comparison between electric discharges in gaseous and liquid dielectric media. Procedia CIRP. 2018;68:330–5. doi:10.1016/j.procir.2017.12.073.
14. Ming W, Zhang S, Zhang G, Du J, Ma J, He W, et al. Progress in modeling of electrical discharge machining process. Int J Heat Mass Transf. 2022;187(1):122563. doi:10.1016/j.ijheatmasstransfer.2022.122563.

15. Yue X, Yang X, Li Q, Li X. Novel methods for high-speed observation of material removal and molten pool movement in EDM. Precis Eng. 2020;66(2):295–305. doi:10.1016/j.precisioneng.2020.07.009.
16. Zhang G, Guo J, Ming W, Huang Y, Shao X, Zhang Z. Study of the machining process of nano-electrical discharge machining based on combined atomistic-continuum modeling method. Appl Surf Sci. 2014;290:359–67. doi:10.1016/j.apsusc.2013.11.084.
17. Shitara T, Fujita K, Yan J. Direct observation of discharging phenomena in vibration-assisted micro-electrical discharge machining. Int J Adv Manuf Technol. 2020;108(4):1125–38. doi:10.1007/s00170-019-04877-7.
18. Li G, Natsu W, Yu Z. Elucidation of gap area phenomenon in micro EDM drilling through direct observation. Procedia CIRP. 2020;95(13):210–4. doi:10.1016/j.procir.2020.02.329.
19. Page MJ, McKenzie JE, Bossuyt PM, Boutron I, Hoffmann TC, Mulrow CD, et al. The PRISMA, 2020 statement: an updated guideline for reporting systematic reviews. BMJ. 2021;372:n71. doi:10.1136/bmj.n71.
20. Hasan MM, Saleh T, Sophian A, Rahman MA, Huang T, Mohamed Ali MS. Experimental modeling techniques in electrical discharge machining (EDM): a review. Int J Adv Manuf Technol. 2023;127(5):2125–50. doi:10.1007/s00170-023-11603-x.
21. Mohd Abbas N, Solomon DG, Bahari MF. A review on current research trends in electrical discharge machining (EDM). Int J Mach Tools Manuf. 2007;47(7–8):1214–28. doi:10.1016/j.ijmachtools.2006.08.026.
22. Banu A, Ali MY. Electrical discharge machining (EDM): a review. Int J Eng Mater Manuf. 2016;1(1):3–10. doi:10.26776/ijemm.01.01.2016.02.
23. Kaigude AR, Khedkar NK, Jatti VS, Salunkhe S, Cep R, Nasr EA. Surface roughness prediction of AISI D2 tool steel during powder mixed EDM using supervised machine learning. Sci Rep. 2024;14(1):9683. doi:10.1038/s41598-024-60543-3.
24. Kamenskikh AA, Muratov KR, Shlykov ES, Sidhu SS, Mahajan A, Kuznetsova YS, et al. Recent trends and developments in the electrical discharge machining industry: a review. J Manuf Mater Process. 2023;7(6):204. doi:10.3390/jmmp7060204.
25. Fu H, Wang S, Song T, Xiong W, Liu X, Xu K, et al. Preparation of high-energy Al-Li alloy powders with enhanced compatibility and combustion performance by dense fluorosilane polymer composite coating. Appl Surf Sci. 2024;673:160788. doi:10.1016/j.apsusc.2024.160788.
26. Yin M, Tang J, Li Z, Yue X, Peng W, Qiu Z, et al. Thermo-hydraulic-metallographic modeling and study of the thermotropic metamorphic layer in EDM of Ti–6Al–4V. J Phys D Appl Phys. 2025;58(2):025305. doi:10.1088/1361-6463/ad800c.
27. Zhao Y, Kunieda M, Abe K. EDM mechanism of single crystal SiC with respect to thermal, mechanical and chemical aspects. J Mater Process Technol. 2016;236(7):138–47. doi:10.1016/j.jmatprotec.2016.05.010.
28. Ming W, Jia H, Zhang H, Zhang Z, Liu K, Du J, et al. A comprehensive review of electric discharge machining of advanced ceramics. Ceram Int. 2020;46(14):21813–38. doi:10.1016/j.ceramint.2020.05.207.
29. Schubert A, Zeidler H, Kühn R, Hackert-Oschätzchen M. Microelectrical discharge machining: a suitable process for machining ceramics. J Ceram. 2015;2015(1):470801. doi:10.1155/2015/470801.
30. Singh H. Experimental study of distribution of energy during EDM process for utilization in thermal models. Int J Heat Mass Transf. 2012;55(19–20):5053–64. doi:10.1016/j.ijheatmasstransfer.2012.05.004.
31. Yeo SH, Kurnia W, Tan PC. Critical assessment and numerical comparison of electro-thermal models in EDM. J Mater Process Technol. 2008;203(1–3):241–51. doi:10.1016/j.jmatprotec.2007.10.026.
32. Xie B, Hou J, Dong B, Xu C, Yao R, Zhang Y. Thermal model of crater formation process in electrical discharge machining. Case Stud Therm Eng. 2024;56(18):104303. doi:10.1016/j.csite.2024.104303.
33. Tang J, Li Z, Yue X. Numerical analysis of plasma channel characteristics and dynamic effects on molten pool in electrical discharge machining. Precis Eng. 2024;86(2):305–16. doi:10.1016/j.precisioneng.2023.12.015.
34. Chen Z, Wu C, Zhou H, Yan H. A new thermal model for predicted discharge craters in micro/nano-EDM considering the non-Fourier effect. Crystals. 2022;12(6):794. doi:10.3390/cryst12060794.
35. Shao B, Rajurkar KP. Modelling of the crater formation in micro-EDM. Procedia CIRP. 2015;33:376–81. doi:10.1016/j.procir.2015.06.085.

36. Gong S, Hu Y, Zhang L, Wang Z, Wang Y. Methodology for surface reconstruction and prediction based on the electrical discharge machining removal mechanism of C(f)-UHTC materials. Materials. 2025;18(2):371. doi:10.3390/ma18020371.
37. Izquierdo B, Sánchez JA, Plaza S, Pombo I, Ortega N. A numerical model of the EDM process considering the effect of multiple discharges. Int J Mach Tools Manuf. 2009;49(3–4):220–9. doi:10.1016/j.ijmachtools.2008.11.003.
38. Joshi SN, Pande SS. Thermo-physical modeling of die-sinking EDM process. J Manuf Process. 2010;12(1):45–56. doi:10.1016/j.jmapro.2010.02.001.
39. Yue X, Yang X. Molecular dynamics simulation of machining properties of polycrystalline copper in electrical discharge machining. Proc Inst Mech Eng Part B J Eng Manuf. 2019;233(2):371–80. doi:10.1177/0954405417748187.
40. Yu Y, Dong S, Liu F, Cui Z, Hou X, An L. A review of advances in electrical discharge machining: from flow field to multi-physics coupled simulations. Results Eng. 2025;27:106631. doi:10.1016/j.rineng.2025.106631.
41. Li Q, Yang X. Study on arc plasma movement and its effect on crater morphology during single-pulse discharge in EDM. Int J Adv Manuf Technol. 2020;106(11):5033–47. doi:10.1007/s00170-020-04964-0.
42. Liu C, Li Q, Yang X. Analysis of arc plasma characteristics and energy distribution in EDM based on two-temperature model. Precis Eng. 2023;83:204–15. doi:10.1016/j.precisioneng.2023.06.008.
43. Tao J, Ni J, Shih AJ. Modeling of the anode crater formation in electrical discharge machining. J Manuf Sci Eng. 2012;134(1):011002. doi:10.1115/1.4005303.
44. Pachaury Y, Tandon P. Electro-thermal modelling for material removal study in electric discharge machining process. In: Proceedings of the ASME 2015 International Mechanical Engineering Congress and Exposition; 2015 Nov 13–19; Houston, TX, USA. New York, NY, USA: American Society of Mechanical Engineers; 2015. doi:10.1115/imece2015-50860.
45. Abdel-Hamid B. Modelling non-Fourier heat conduction with periodic thermal oscillation using the finite integral transform. Appl Math Model. 1999;23(12):899–914. doi:10.1016/S0307-904X(99)00017-7.
46. Kulkarni A, Dongre G. Comparative study of statistical and soft computing approaches for forecasting material removal rate and temperature in the EDM process of Inconel 718. Discov Mech Eng. 2025;4(1):62. doi:10.1007/s44245-025-00156-w.
47. Li Q, Yang X. Modelling and simulation of surface formation in electrical discharge machining based on thermo-hydraulic coupling. Precis Eng. 2024;85(7):126–35. doi:10.1016/j.precisioneng.2023.09.013.
48. Zhang W, Chang H, Liu Y. Study on solidification process and residual stress of SiCp/Al composites in EDM. Micromachines. 2022;13(6):972. doi:10.3390/mi13060972.
49. Zhang S, Zhang W, Chang H, Liu Y, Ma F, Yang D, et al. Study of the thermal erosion, ejection and solidification processes of electrode materials during EDM. Eng Appl Comput Fluid Mech. 2019;13(1):1153–64. doi:10.1080/19942060.2019.1676313.
50. Alshaer AW, Rogers BD, Li L. Smoothed Particle Hydrodynamics (SPH) modelling of transient heat transfer in pulsed laser ablation of Al and associated free-surface problems. Comput Mater Sci. 2017;127:161–79. doi:10.1016/j.commatsci.2016.09.004.
51. Papazoglou EL, Karmiris-Obratański P, Karkalos NE, Markopoulos AP. On the use of deformed geometry in EDM modelling: comparative study. Acta Phys Pol A. 2020;138(2):268–71. doi:10.12693/aphyspola.138.268.
52. Papazoglou EL, Karmiris-Obratański P, Karkalos NE, Thangaraj M, Markopoulos AP. Theoretical and experimental analysis of plasma radius expansion model in EDM: a comprehensive study. Int J Adv Manuf Technol. 2023;126(5):2429–44. doi:10.1007/s00170-023-11292-6.
53. Qin L, Huo W, Li Z, Zhang YO, Xi X, Zhao W. Study on energy distribution of discharge plasma and its effect on crater formation in EDM. Int J Adv Manuf Technol. 2022;121(7):5563–85. doi:10.1007/s00170-022-09755-3.
54. Raza S, Kishore H, Nirala CK, Rajurkar KP. Multiphysics modelling and high-speed imaging-based validation of discharge plasma in micro-EDM. CIRP J Manuf Sci Technol. 2023;43:15–29. doi:10.1016/j.cirpj.2023.02.006.
55. Raza S, Nirala CK. Multiphysics simulation of plasma channel formation during micro-electrical discharge machining. AIP Adv. 2021;11(2):025138. doi:10.1063/5.0028665.
56. Qin L, Huo WJ, Hu J, Wang J, Zhao WS, Zhang YO. A parallel PIC-MCC simulation of microsecond discharge modeling in EDM. Int J Adv Manuf Technol. 2022;119(7):5467–81. doi:10.1007/s00170-021-08510-4.

57. Hinduja S, Kunieda M. Modelling of ECM and EDM processes. CIRP Ann. 2013;62(2):775–97. doi:10.1016/j.cirp.2013.05.011.
58. Alshaer AW, Abdallah R, Rajab FH, Barzinjy AA, Otanocha OB. Understanding the machined material's behaviour in electro-discharge machining (EDM) using a multi-phase smoothed particle hydrodynamics (SPH) modelling. Int J Adv Manuf Technol. 2024;134(1):369–87. doi:10.1007/s00170-024-14116-3.
59. Shabgard M, Ahmadi R, Seyedzavvar M, Oliaei SNB. Mathematical and numerical modeling of the effect of input-parameters on the flushing efficiency of plasma channel in EDM process. Int J Mach Tools Manuf. 2013;65(5):79–87. doi:10.1016/j.ijmachtools.2012.10.004.
60. Tlili A, Ghanem F, Ben Salah N. A contribution in EDM simulation field. Int J Adv Manuf Technol. 2015;79(5–8):921–35. doi:10.1007/s00170-015-6880-1.
61. Chu X, Zhu K, Wang C, Hu Z, Zhang Y. A study on plasma channel expansion in micro-EDM. Mater Manuf Process. 2016;31(4):381–90. doi:10.1080/10426914.2015.1059445.
62. Escobar AM, de Lange DF, Medellín Castillo HI. Simplified plasma channel formation model for the electrical discharge machining process. Int J Adv Manuf Technol. 2020;106(1):143–53. doi:10.1007/s00170-019-04593-2.
63. Sahoo R, Singh NK, Bajpai V. A novel approach for modeling MRR in EDM process using utilized discharge energy. Mech Syst Signal Process. 2023;185(13):109811. doi:10.1016/j.ymssp.2022.109811.
64. Gholipoor A, Shabgard MR, Mohammadpourfard M. A novel approach to plasma channel radius determination and numerical modeling of electrical discharge machining process. J Braz Soc Mech Sci Eng. 2020;42(4):185. doi:10.1007/s40430-020-2244-3.
65. Trelles JP. Fluid modeling of low-temperature plasmas. Phys Plasmas. 2025;32(9):090901. doi:10.1063/5.0270714.
66. Reza M, Faraji F, Knoll A. Latest progress on the reduced-order particle-in-cell scheme: I. Refining the underlying formulation. Plasma Phys Control Fusion. 2025;67(8):085008. doi:10.1088/1361-6587/adef78.
67. Zinchenko A, Fernandez-Gamiz U, Redchyts D, Gorna O, Bilousova T. An efficient parallelization technique for the coupled problems of fluid, gas and plasma mechanics in the grid environment. Sci Rep. 2025;15(1):8629. doi:10.1038/s41598-025-91695-5.
68. Crouseilles N, Liu H, Yue Y. Semi-lagrangian SAV method for Vlasov-Maxwell equations. J Comput Phys. 2026;549(10):114606. doi:10.1016/j.jcp.2025.114606.
69. Quan L, Cao Y, Li Y, Liu H, Tian B. Influence of the axial oscillations on the electron cyclotron drift instability and electron transport in Hall thrusters. Phys Plasmas. 2023;30(4):043510. doi:10.1063/5.0134644.
70. Baldry M, Haidar LL, Akhavan B, Bilek MMM. Continuum modelling of an asymmetric CCRF *Argon* plasma reactor: influence of higher excited states and sensitivity to model parameters. Plasma Process Polym. 2021;18(6):2000243. doi:10.1002/ppap.202000243.
71. Tanveer A, Kapoor SG, Mujumdar S, Curreli D. One-dimensional plasma model of electrical discharge machining in deionized water for prediction of plasma characteristics along the interelectrode gap. J Manuf Sci Eng. 2023;145(1):011012. doi:10.1115/1.4056265.
72. Mujumdar S, Bayki S. 0D modeling of dry-electrical discharge machining plasma discharge. J Micro Nano Manuf. 2023;11(1):011001. doi:10.1115/1.4064105.
73. Ho A, Datta IAM, Shumlak U. Physics-based-adaptive plasma model for high-fidelity numerical simulations. Front Phys. 2018;6:105. doi:10.3389/fphy.2018.00105.
74. Longmire NP, Banuti DT. Limits of fluid modeling for high pressure flow simulations. Aerospace. 2022;9(11):643. doi:10.3390/aerospace9110643.
75. Ezzatneshan E, Vaseghnia H. Evaluation of equations of state in multiphase lattice Boltzmann method with considering surface wettability effects. Phys A Stat Mech Appl. 2020;541(1):123258. doi:10.1016/j.physa.2019.123258.
76. Assarzadeh S, Ghoreishi M. Electro-thermal-based finite element simulation and experimental validation of material removal in static gap single-spark die-sinking electro-discharge machining process. Proc Inst Mech Eng Part B J Eng Manuf. 2017;231(1):28–47. doi:10.1177/0954405415572661.
77. Shi EL, Hammett GW, Stoltzfus-Dueck T, Hakim A. Gyrokinetic continuum simulation of turbulence in a straight open-field-line plasma. J Plasma Phys. 2017;83(3):905830304. doi:10.1017/s002237781700037x.

78. Bradshaw K, Srinivasan B. Energy-dependent implementation of secondary electron emission models in continuum kinetic sheath simulations. Plasma Sources Sci Technol. 2024;33(3):035008. doi:10.1088/1361-6595/ad331c.
79. Degond P, Deluzet F. Asymptotic-Preserving methods and multiscale models for plasma physics. J Comput Phys. 2017;336(1):429–57. doi:10.1016/j.jcp.2017.02.009.
80. Razeghiyadaki A, Molardi C, Talamona D, Perveen A. Modeling of material removal rate and surface roughness generated during electro-discharge machining. Machines. 2019;7(2):47. doi:10.3390/machines7020047.
81. Weingärtner E, Kuster F, Wegener K. Modeling and simulation of electrical discharge machining. Procedia CIRP. 2012;2:74–8. doi:10.1016/j.procir.2012.05.043.
82. Papazoglou EL, Karmiris-Obratański P, Leszczyńska-Madej B, Markopoulos AP. A study on electrical discharge machining of titanium Grade2 with experimental and theoretical analysis. Sci Rep. 2021;11(1):8971. doi:10.1038/s41598-021-88534-8.
83. Wang L, Xu J, Wang J. A peridynamic framework and simulation of non-Fourier and nonlocal heat conduction. Int J Heat Mass Transf. 2018;118(15–16):1284–92. doi:10.1016/j.ijheatmasstransfer.2017.11.074.
84. Yue X, Yang X. Molecular dynamics simulation of material removal process and mechanism of EDM using a two-temperature model. Appl Surf Sci. 2020;528:147009. doi:10.1016/j.apsusc.2020.147009.
85. Li Q, Yang X. Thermo-hydraulic analysis of melt pool dynamics and material removal on anode in electrical discharge machining. Int J Heat Mass Transf. 2023;203(7–8):123816. doi:10.1016/j.ijheatmasstransfer.2022.123816.
86. Algodi SJ, Clare AT, Brown PD. Modelling of single spark interactions during electrical discharge coating. J Mater Process Technol. 2018;252:760–72. doi:10.1016/j.jmatprotec.2017.10.029.
87. Chen J, Gu L, Zhao W, Guagliano M. Simulation of temperature distribution and discharge crater of SiCp/Al composites in a single-pulsed arc discharge. Chin J Aeronaut. 2021;34(9):37–46. doi:10.1016/j.cja.2020.05.033.
88. Ahmed A, Fardin A, Tanjilul M, Wong YS, Rahman M, Senthil Kumar A. A comparative study on the modelling of EDM and hybrid electrical discharge and arc machining considering latent heat and temperature-dependent properties of Inconel 718. Int J Adv Manuf Technol. 2018;94(5):2729–37. doi:10.1007/s00170-017-1100-9.
89. Yang X, Lu S, Li X, Li Q. Discharge crater formation simulation coupled by thermo-fluid analysis of arc plasma in EDM. Procedia CIRP. 2020;95(3):232–7. doi:10.1016/j.procir.2020.02.253.
90. Koyano T, Yasue T, Furumoto T. Thermo-fluid analysis and experimental investigation of the effects of discharge current waveforms on formation of discharge craters in electrical discharge machining. Int J Electr Mach. 2025;30:23. doi:10.2526/ijem.30.23.
91. Zhang C, Cheng P, Cao J. Mesoscale simulation of Marangoni convection about a vapor bubble in a liquid with temperature gradients under microgravity conditions. Int Commun Heat Mass Transf. 2016;78(3):295–303. doi:10.1016/j.icheatmasstransfer.2016.09.005.
92. Tang J, Yang X. A thermo-hydraulic modeling for the formation process of the discharge crater in EDM. Procedia CIRP. 2016;42(3):685–90. doi:10.1016/j.procir.2016.02.302.
93. Rajhi W, Boujelbene M, Ben Said L, Subhani T, Khaliq A, El Aoud B, et al. Study of the effect of spark radius model upon the performance characteristics in EDM process. J Manuf Process. 2024;124(8):282–99. doi:10.1016/j.jmapro.2024.05.083.
94. Wang T, Zhe J, Zhang YQ, Li YL, Wen XR. Thermal and fluid field simulation of single pulse discharge in dry EDM. Procedia CIRP. 2013;6:427–31. doi:10.1016/j.procir.2013.03.032.
95. Rana P, Bhartiya D, Marla D. Modeling of thermal damage and residual stress in slicing of silicon wafers using wire-electrical discharge machining: comparison with experiments. J Manuf Process. 2023;85(1–3):69–79. doi:10.1016/j.jmapro.2022.10.079.
96. Tan TH, Yan J. Atomic-scale characterization of subsurface damage and structural changes of single-crystal silicon carbide subjected to electrical discharge machining. Acta Mater. 2017;123:362–72. doi:10.1016/j.actamat.2016.10.045.
97. Soori M, Jough FKG. Minimization of residual stress, surface roughness and tool wear in electro discharge machining of inconel 625. J Eng Res. 2025;13(3):1843–53. doi:10.1016/j.jer.2024.05.028.
98. Liu JF, Guo YB. Residual stress modeling in electric discharge machining (EDM) by incorporating massive random discharges. Procedia CIRP. 2016;45:299–302. doi:10.1016/j.procir.2016.02.060.

99. Ekmekci B, Tekkaya AE, Erden A. A semi-empirical approach for residual stresses in electric discharge machining (EDM). Int J Mach Tools Manuf. 2006;46(7–8):858–68. doi:10.1016/j.ijmachtools.2005.07.020.
100. Schneider S, Vorspohl J, Frerichs F, Klink A, Meinke M, Schröder W, et al. Investigation on residual stress induced by multiple EDM discharges. Procedia CIRP. 2021;102(2):482–7. doi:10.1016/j.procir.2021.09.082.
101. Patil D, Kuriachen B, Mathew J. Modeling and experimental validation of residual stress distribution during micro-electro discharge machining of titanium alloy. J Manuf Sci. 2022;11(1):8–15.
102. Paswan K, Sharma S, Li C, Mohammed KA, Kumar A, Abbas M, et al. Unravelling the analysis of electrical discharge machining process parameters, microstructural morphology, surface integrity, recast layer formation, and material properties: a comparative study of aluminum, brass, and Inconel 617 materials. J Mater Res Technol. 2023;27(5):7713–29. doi:10.1016/j.jmrt.2023.11.186.
103. Ramasawmy H, Blunt L, Rajurkar KP. Investigation of the relationship between the white layer thickness and 3D surface texture parameters in the die sinking EDM process. Precis Eng. 2005;29(4):479–90. doi:10.1016/j.precisioneng.2005.02.001.
104. Rebelo JC, Morao Dias A, Kremer D, Lebrun JL. Influence of EDM pulse energy on the surface integrity of martensitic steels. J Mater Process Technol. 1998;84(1–3):90–6. doi:10.1016/S0924-0136(98)00082-X.
105. Lalwani V, Sharma P, Pruncu CI, Unune DR. Response surface methodology and artificial neural network-based models for predicting performance of wire electrical discharge machining of inconel 718 alloy. J Manuf Mater Process. 2020;4(2):44. doi:10.3390/jmmp4020044.
106. Sana M, Asad M, Farooq MU, Anwar S, Talha M. Machine learning for multi-dimensional performance optimization and predictive modelling of nanopowder-mixed electric discharge machining (EDM). Int J Adv Manuf Technol. 2024;130(11):5641–64. doi:10.1007/s00170-024-13023-x.
107. Ugrasen G, Ravindra HV, Naveen Prakash GV, Keshavamurthy R. Process optimization and estimation of machining performances using artificial neural network in wire EDM. Procedia Mater Sci. 2014;6:1752–60. doi:10.1016/j.mspro.2014.07.205.
108. Sana M, Farooq MU, Anwar S, Haber R. Predictive modelling framework on the basis of artificial neural network: a case of nano-powder mixed electric discharge machining. Heliyon. 2023;9(12):e22508. doi:10.1016/j.heliyon.2023.e22508.
109. Pant P, Bharti PS. Bi-Objective predictive modelling and optimization in micro-electrical discharge machining process using an artificially intelligent system. Eng Appl Artif Intell. 2025;143(2):109975. doi:10.1016/j.engappai.2024.109975.
110. Ghadai R, Kalita K, Gao XZ. Symbolic regression metamodel based multi-response optimization of EDM process. FME Trans. 2020;48(2):404–10. doi:10.5937/fme2002404g.
111. Somani N, Singh Walia A, Kumar Gupta N, Prakash Panda J, Das A, Ranjan Das S. Data driven surrogate model-based optimization of the process parameters in electric discharge machining of D2 steel using Cu-SiC composite tool for the machined surface roughness and the tool wear. Rev Metal. 2023;59(2):e242. doi:10.3989/revmetalm.242.
112. Singh NK, Singh Y, Kumar S, Upadhyay R. Integration of GA and neuro-fuzzy approaches for the predictive analysis of gas-assisted EDM responses. SN Appl Sci. 2019;2(1):137. doi:10.1007/s42452-019-1533-x.
113. Singh NK, Upadhyay RK, Singh Y, Sharma A. Intelligent hybrid approaches for ensuring better prediction of gas-assisted EDM responses. SN Appl Sci. 2020;2(5):914. doi:10.1007/s42452-020-2654-y.
114. Sana M, Asad M, Farooq MU, Tlija M, Haber R. Sustainability metrics targeted optimization and electric discharge process modelling by neural networks. Sci Rep. 2025;15(1):3375. doi:10.1038/s41598-024-78883-5.
115. Ilani MA, Banad YM. EDMNet: unveiling the power of machine learning in regression modeling of powder mixed-EDM. Int J Adv Manuf Technol. 2024;135(5):2555–70. doi:10.1007/s00170-024-14686-2.
116. Abaza BF, Gheorghita V. Artificial neural network framework for Hybrid control and monitoring in turning operations. Appl Sci. 2025;15(7):3499. doi:10.3390/app15073499.
117. Zhou M, Jing H, Yang J, Yao S, He L. An extended adaptive control system for EDM. Procedia CIRP. 2018;68(3):672–7. doi:10.1016/j.procir.2017.12.152.

118. Dwaraka R, Arunachalam N. Investigation on non-invasive process monitoring of Die Sinking EDM using Acoustic Emission signals. Procedia Manuf. 2018;26(2):1471–82. doi:10.1016/j.promfg.2018.07.094.
119. Tejas VR, Venkatesh Raju NR, Vishnu Prasad N, Gowda MKY, Irfanulla M, Naik GM. Hybrid ensemble learning with uncertainty quantification for multi-objective EDM parameter optimization. J Eng Res Rep. 2025;27(11):503–20. doi:10.9734/jerr/2025/v27i111718.
120. Saha S, Gupta KK, Maity SR, Dey S. Data-driven probabilistic performance of Wire EDM: a machine learning based approach. Proc Inst Mech Eng Part B J Eng Manuf. 2022;236(6–7):908–19. doi:10.1177/09544054211056417.
121. Sundaram M, Jamunkar T, Rajurkar K. Digital twin modeling of surface texture generation by the electrical discharge machining process. Procedia CIRP. 2025;137(1):7–12. doi:10.1016/j.procir.2025.03.077.
122. de Almeida ST, Mo JPT, Bil C, Ding S, Cheng CT. Accurate EDM calibration of a digital twin for a seven-axis robotic EDM system and 3D offline cutting path. Micromachines. 2025;16(8):892. doi:10.3390/mi16080892.
123. Hsue AW, Fu WZ, Lin GW. Iterative monitoring of wire-EDM stability through pulses energy distribution and a K-means regression model. Procedia CIRP. 2025;137:323–8. doi:10.1016/j.procir.2025.03.078.
124. Liu JF, Guo YB. Modeling of white layer formation in electric discharge machining (EDM) by incorporating massive random discharge characteristics. Procedia CIRP. 2016;42:697–702. doi:10.1016/j.procir.2016.02.304.
125. Luis-Pérez CJ, Torres-Salcedo A, Puertas-Arbizu I. Optimization and modeling of ZrB_2 ceramic processing by EDM for high-performance industrial applications. J Mater Res Technol. 2025;36(6):3486–508. doi:10.1016/j.jmrt.2025.03.088.
126. Ulhakim MT, Sukarman, Khoirudin, Mulyadi D, Susilo H, Rohman, et al. Electrical discharge machining: recent advances and future trends in modeling, optimization, and sustainability. Int J Light Mater Manuf. 2025;8(4):495–511. doi:10.1016/j.ijlmm.2025.03.006.
127. Su G, Zhang C, Li J, Chen X, Liu G, Zhang Y. Plasma characteristics and material erosion mechanism in multi-channel wire electrical discharge machining. Chin J Aeronaut. 2024;37(10):508–25. doi:10.1016/j.cja.2024.02.025.
128. Cheng C, Liu B, Cheng J, Xiong X. A novel physically guided data fusion prediction model for micro-EDM drilling. Materials. 2023;16(23):7454. doi:10.3390/ma16237454.
129. Trzepieciński T, Dell'Isola F, Lemu HG. Multiphysics modeling and numerical simulation in computer-aided manufacturing processes. Metals. 2021;11(1):175. doi:10.3390/met11010175.
130. Jebahi M, Dau F, Charles JL, Iordanoff I. Multiscale modeling of complex dynamic problems: an overview and recent developments. Arch Comput Meth Eng. 2016;23(1):101–38. doi:10.1007/s11831-014-9136-6.
131. Radhakrishnan R. A survey of multiscale modeling: foundations, historical milestones, current status, and future prospects. AIChE J. 2021;67(3):e17026. doi:10.1002/aic.17026.
132. Sheuly SS, Ahmed MU, Begum S. Machine-learning-based digital twin in manufacturing: a bibliometric analysis and evolutionary overview. Appl Sci. 2022;12(13):6512. doi:10.3390/app12136512.
133. Abhilash PM, Boban J, Ahmed A, Luo X. Digital twin-driven additive manufacturing. In: Hybrid metal additive manufacturing. Boca Raton, FL, USA: CRC Press; 2023. p. 196–221. doi:10.1201/9781003406488-12.